CZECH TECHNICAL UNIVERSITY IN PRAGUE
FACULTY OF MECHANICAL ENGINEERING

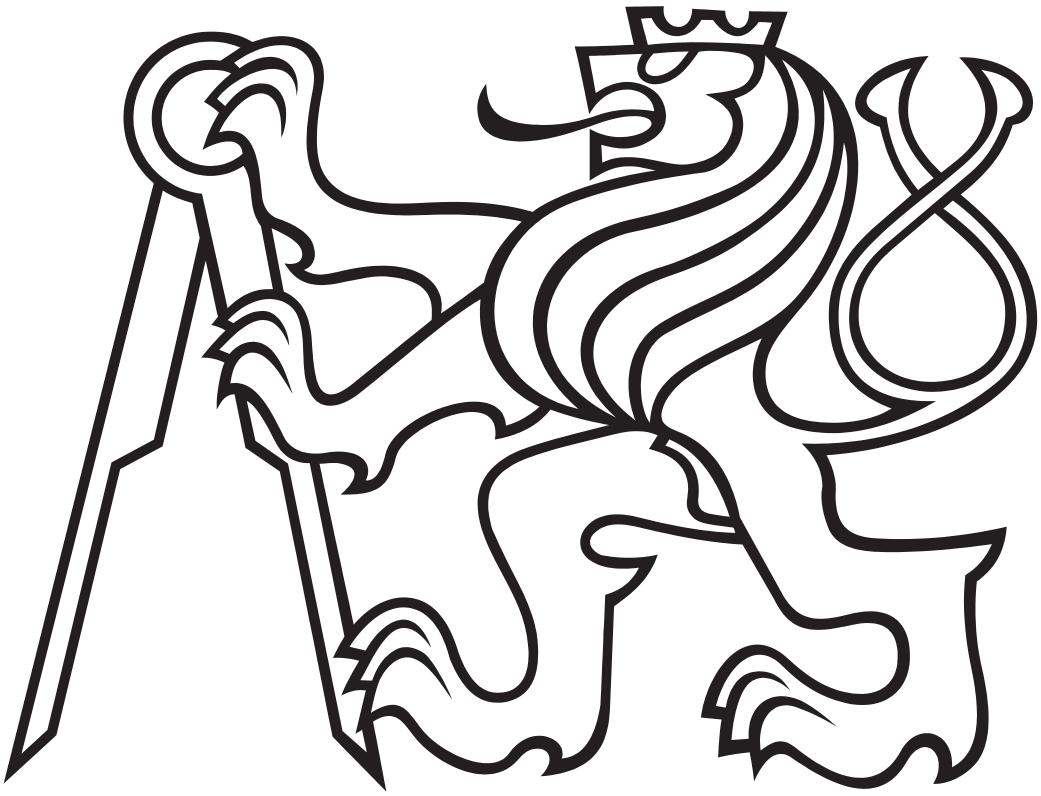

DOCTORAL THESIS STATEMENT

Czech Technical University in Prague
Faculty of Mechanical Engineering
Department of Technical Mathematics

Doctoral thesis statement

NUMERICAL SIMULATION OF FLUID-STRUCTURE-ACOUSTIC INTERACTION IN HUMAN PHONATION

Ing. Jan Valášek

Doctoral study programme: Mechanical Engineering

Branch of study: Mathematical and Physical Engineering

Supervisor: Doc. RNDr. Petr Sváček, Ph.D.

A doctoral thesis statement submitted for the degree of "Doctor", abbreviated to "Ph.D."

Prague, 2021

The doctoral thesis was produced during a Ph.D. study in a full-time internal form at the Department of Technical Mathematics of the Faculty of Mechanical Engineering of the Czech Technical University in Prague.

Candidate: Ing. Jan Valášek
Department of Technical Mathematics, Faculty of Mechanical Engineering, CTU in Prague
Karlovo náměstí 13, 121 35 Prague 2

Supervisor: Doc. RNDr. Petr Sváček, Ph.D.
Department of Technical Mathematics, Faculty of Mechanical Engineering, CTU in Prague
Karlovo náměstí 13, 121 35 Prague 2

Opponents:

The doctoral thesis statement was distributed on: .....

The defence of the doctoral thesis will be held on ..... at ..... a.m./p.m. before the Board for the Defence of the Doctoral Thesis in the branch of study Mathematical and Physical Engineering in the meeting room No. ..... of the Faculty of Mechanical Engineering of the CTU in Prague.

Those interested may get acquainted with the doctoral thesis concerned at the Department for Science and Research of the Faculty of Mechanical Engineering of the CTU in Prague, Technická 4, Prague 6.

Doc. Ing. Jiří Fürst, Ph.D.

Chairman of the Board for the Defence of the Doctoral Thesis in the branch of study Mathematical and Physical Engineering

Faculty of Mechanical Engineering, CTU in Prague

Table of contents

1 Introduction

Fluid-structure-acoustic interaction (FSAI) is a coupled problem, where three different physical fields – the deformation of an elastic body, the complex fluid flow and the acoustics, interact together. Thus it is important to consider all their mutual couplings. Typical technical problems involving FSAI are e.g. design of ventilators, air-conditioning vents or engines, [31], [47], where the FSAI simulation can help already in first stages of design to reduce significantly the sound emission. The simulation of human phonation is a prominent example of other than purely technical application, [38], [48].

In this work the FSAI solution is sought with the help of mathematical modelling and numerical approximation by the finite element method (FEM), particularly, specialized (and therefore more efficient) solver for solution of each subproblem is used. The aim of the work is to apply all derived methodology to the simulation of human phonation. Due to the practical inaccessibility of the human vocal folds (VFs) for experimental investigations, the mathematical modelling have become to be an important tool used in the research, see e.g. [56].

Human voice creation starts by pressurized air stream exciting vibrations of VFs. If the subglottal pressure is high enough, the amplitude of vibration steeply rises until the contact of both VFs is achieved. The complete closure of the glottal channel is one of the major characteristics of the healthy human voice, [56], [40]. The basic sound is created by modulated glottal jet with the fundamental frequency given by the VFs vibration. This dominant sound is enriched by sound sources associated with supraglottal turbulence vortices and sound sources introduced by the VF vibration and collision, however the frequency characteristic of sound sources is still substantially different from produced human voice, see [56], [57].

The sound originated at the glottis propagates through vocal tract and then it is articulated in mouth and this acoustic signal create a human voice as we know it. The basic physical conception of vocal tract function is, that it acts as an acoustic resonator with associated resonant frequencies, see source-filter theory in e.g. [56]. It means that it amplifies frequencies in specific frequency ranges given by acoustic resonances of the vocal tract. By doing so, it effectively transforms basic sound produced in the glottis into acoustic frequencies typical for each vowel.

State of the art

For overall FSAI simulation accuracy is very important to appropriately approximate fluid flow part of the problem described by the nonlinear convection-dominated partial differential equations (PDE) which need to be stabilized. In order to take into account the dynamical effects caused by the flow domain change commonly used finite volume method (FVM) or FEM are usually further modified. One of most popular and most straightforward way provides the arbitrary Lagrangian-Eulerian (ALE) method, see [53] or in a conjuction with the FEM see [23], [24] and with the FVM see [48], [43], although many other approaches like immersed boundary method - see [47], [58], or others - see e.g. [46], exist. A separate chapter represents the numerical construction of the ALE mapping, i.e. bijective mapping from the reference flow domain to a deformed one, can be constructed by many strategies, e.g. the algebraic mesh motion, the elliptic smoothing, see [38], the interpolation by radial basis functions (RBF), see [41], or the pseudo-elastic approach, see [33].
Further, in the supraglottal fluid field complex flow structures appears and possibly turbulence effects should be considered. However, most turbulence models are usually well tuned to describe the fluid flow around an airfoil or plane wall and a choice of turbulence model, which gives also good results for the case with massive separations, is troublesome see [36]. Thus most promising approach in this area seems to be the application of LES models, see [50], [36] or [43].

Next step towards human phonation simulation is a reliable numerical simulation of fluid-structure interaction (FSI) problem. One of the first FSI continuum model of flow-induced

VF vibration approximated by the FEM was introduced in [42]. This approach is still used in many studies, e.g. [54], [23] or [51] as it provides high accuracy, although recently also the discountinous Galerkin (DG) methods can be found, see e.g. [35].
Since the solution of full FSI problem is highly computationally expensive, a simplified approach is often used. Then a variously complicated motion of fluid domain walls is prescribed in order to imitate the real VF motion in 2D computations, see [59], [18], or for 3D case see [48], [43].

Definition of boundary conditions (BCs) is a neccessary part of the problem formulation. For the interface between the fluid and the structure the combination of the Dirichlet and the Neumann BC is commonly used, [61], albeit a combination of the Robin-Robin BCs can possibly accelerate the convergence rate, [17]. Next, we focus on the inlet BCs for incompressible Navier-Stokes equations in the FEM framework as their influence is significant because the neccesity to model the periodic closure of the glottal channel. There are two frequently used inlet BCs: The Dirichlet condition prescribing inlet velocity has the drawback of high, unphysical oscillations of inlet pressure values during the channel closing phase, see [52], and the do-nothing type of BC with a given pressure drop between the inlet and the outlet usually leads to significant oscillation of the inlet velocity while keeping the pressure drop constant. Also such a behaviour is not relevant for the considered problem, i.e. it was not observed experimentally - see [27]. A remedy for this situation seems to be penalization approach with the idea proposed already in [16] for a scalar problem. Its potential for this configuration of inner fluid dynamics was newly discovered in [52]. The penalization approach imposes the inlet boundary conditions inside the weak formulation with a penalization parameter ϵ.

Aeroacoustics. The aeroacoustics is a part of acoustics with the aim to desribe the flow-induced sound, usually produced by flow around obstacles or by a high Reynolds number (turbulent) flow, see e.g. [30]. The first aeroacoustic mathematic model known as Lighthill (LH) acoustic analogy was introduced in 1952, [37]. Acoustic analogy means some approximative transformation of Navier-Stokes equations, which compressible variant in general describes propagation of entropy, vorticity and acoustics, see [22], into PDE similar to wave equation for a representation of acoustic pressure. Ffowcs-Williams Hawkings (FWH) analogy is a generalization of the LH analogy for the case of boundaries presence in a acoustic domain, see [34]. Modern computational aeroacoustics is based on the perturbation equations [34], where the splitting of flow variables into mean, acoustic and correction term is performed with the aim to describe purely acoustic wave propagation. There are a lot formulations, see e.g. [22], [18] and [47]. The splitting approach was later generelized, see [31], leading to approach called the perturbed convective wave equation (PCWE) and the aeroacoustic wave equation (AWE) with practical formulation for low Mach numbers flow regimes, see [44].

The theoretical background of sound production during voicing was described in work [59] using integral FWH analogy and sound sources multipole classification. They found that the most dominant sound source during phonation is a dipole associated with net forces exerted by the surface of the VFs onto the airflow. The other source is a quadrupole connected with turbulence in the supraglottal area and a monopole related to the air column movement induced by VF vibration, see also [50], [48]. In paper [38] the LH analogy was applied using results of 2D FSI simulation. The high order IBM solver was used for solving 3D fluid flow in a static supraglottal region with prescribed time variable flow rate and perturbation equations approach was utilized in [47]. In article [48] the aeroacoustic 3D problem with vocal tract was successfully solved using the LH analogy and the PCWE approach based on the FSI solution with the prescribed movement of VF walls. In the thesis [39] a combination of experimental flow measurements and numerical acoustic simulations are presented.

Numerical simulation of human phonation. The numerical simulations of human phonation using mathematical model of continuum can be basically split in two groups. The studies

from the first group are interested in the solution of FSI problem of flow-induced VF vibration for realistic geometries and they usually do not considered the associated aeroacoustic problem, see [54], [61], [23], [58]. The second group of results deals dominantly with the aeroacoustic treatment usually based on the roughly simplified fluid flow simulation in the glottis and in the larynx. The FSI problem is often reduced by considering a rigid glottal model, [50], typically together with some given fluctuating inlet flow profile, see [47]. Another frequently used reduction of the FSI problem can be realized by prescribing highly simplified VF motion, see [59], [18].

There are few research studies trying to join the both aforementioned approaches with all consequences. First, paper [48] calculated the resulting acoustic signal in front of mouth based on the 3D flow results obtained by FVM with sophisticated prescribed periodic VF motion simulating changing convergent-divergent VF position. They achieved with included model of vocal tract (VT) a good match of vowel spectra [u:] and [i:] with experimental results. Another studies [38], [21], considered the full FSAI problem however they did not provide relevant acoustic results as any VT model was not included.

2 Objectives of dissertation

The aim of this thesis is to simulate the process of human phonation numerically. The exact mathematical formulation of all relevant physical processes together with their mutual interaction must be unquestionable part of this work. Further the numerical schemes based on FEM are adopted, which are capable to simulate all main important involved phenomena. The orientation only on the 2D coupled FSAI problem is caused by enormous rise of computational demand for 3D version. The first two goals concern a numerical solution of the FSI problem.

The first goal is to investigate the possibilities of new penalization boundary condition and to compare it with the other commonly used BCs for the FSI problem with the prescribed as well as unknown VF motion. The sensitivity analysis of the flow and the FSI characteristics on the value of ϵ is highly desired.

The second goal is to (numerically) study the stability boundary of the FSI problem. The knowledge of critical inlet airflow velocity is needed for determination of the start of flow-induced VF vibrations. Flutter velocity is one of the characteristics of the FSI system.

The second part of the thesis addresses the problem of human phonation simulation. According to *State of the art* the extension of the FSI problem to the FSAI problem will be a novel result.

The third goal is to connect the in-house solver FSIFEM of the FSI problem, see [1], and the academic solver CFS++ of the multiphysics problems from TU Vienna. The connection between solvers could be realized through a support of the file format called Hierarchical Data Format.

The fourth goal is to perform the aeroacoustic simulation of human phonation based on the full FSI solution. In order to obtain relevant acoustic results, a vocal tract model needs to be included in the acoustic domain. Further, a comparison of different aeroacoustic formulations could bring more light in their applicability.

The fifth goal is to compare sounds of aeroacoustic and vibroacoustic origin.

Structure of the work

The work is organized as follows: The first and the second section was this introduction and the objectives of the work. The third section contains mathematical description of the FSAI problem with all considered mutual couplings. In the fourth section the numerical methods for FSAI problem based on the FEM are explained. The fifth section is devoted to FSI numerical results with a special attention to the penalization inlet boundary condition. The sixth section presents the acoustic results of numerical simulations of the human phonation. The last seventh section concludes the work with discussion of numerical results and achieved goals.

3 Mathematical model

Here, a simplified two-dimensional model of FSI problem is introduced, see Figure 1, where the reference and the deformed states are shown. For the description of the elastic structure deformation the Lagrange coordinates are utilized, i.e. the computational domain $\Omega^s = \Omega^s_t = \Omega^s_{\mathrm{ref}} \subset \mathbb{R}^2$ at arbitrary time t is used.

The domain $\Omega^f_{\mathrm{ref}} \subset \mathbb{R}^2$ represents the reference fluid domain, e.g. the domain occupied by fluid at the time instant $t = 0$ with the common interface $\Gamma_{\mathrm{W_{ref}}} = \Gamma_{\mathrm{W_0}}$ between the fluid and the structure domain. The deformation of the reference domain Ω^f_{ref} onto the domain $\Omega^f_t \subset \mathbb{R}^2$ occupied by fluid at any time instant $t \in (0, \mathrm{T})$ is determined by the motion of the elastic structure and more specifically by the displacement of the reference interface $\Gamma_{\mathrm{W_{ref}}}$ onto $\Gamma_{\mathrm{W_t}}$. It treated with the aid of the ALE method.

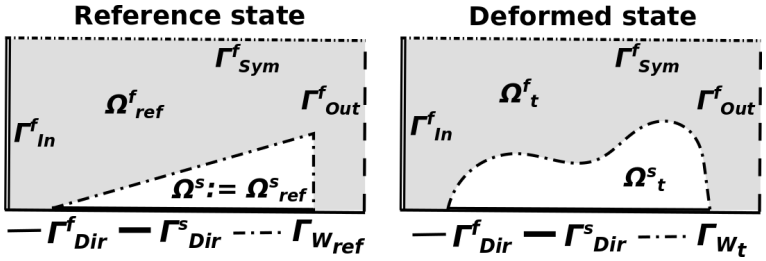

Figure 1: Scheme of FSI configuration in the reference state on the left and in a deformed state at arbitrary time t on the right. The computational domain is composed of the elastic structure domain Ω^s and the fluid domain Ω^f_t together with boundaries: inlet Γ^f_{In}, outlet Γ^f_{Out}, symmetric boundary Γ^f_{Sym}, walls Γ^f_{Dir}, Γ^s_{Dir} and interface Γ_{W}.

3.1 Elastic body

The deformation of the elastic body Ω^s described by a displacement $\mathbf{u}(X,t) = (u_1, u_2),\ X \in \Omega^s$ is governed by equations

$$-\rho^s \frac{\partial^2 u_i}{\partial t^2} + \frac{\partial \tau^s_{ij}}{\partial X_j} + f^s_i = 0, \qquad \text{in } \Omega^s, \tag{1}$$

where ρ^s denotes the elastic body density, the tensor τ_{ij} is the Cauchy stress tensor and the vector $\mathbf{f}^s = (f^s_1, f^s_2)$ represents a volume force density. Let us emphasize that in equation (1) the Einstein summation convection (for $j = 1, 2$) is used. Using the assumption of the linear relation between the deformation and the stress tensor given by the generalized Hooke's law and assuming the isotropic material leads to

$$\tau^s_{ij} = \lambda^s (\operatorname{div} \mathbf{u})\, \delta_{ij} + 2\mu^s e^s_{ij}, \tag{2}$$

where λ^s, μ^s are Lamé coefficients depending on the Young's modulus of elasticity E^s and the Poisson's ratio σ^s, see e.g. [20]. The tensor $\mathbb{I} = (\delta_{ij})$ denotes the Kronecker's delta and tensor $\mathbf{e}^s = (e^s_{ij})$ is the strain tensor. Using small displacements assumption the strain tensor components read, see e.g. [20],

$$e^s_{jk} = \frac{1}{2}\left(\frac{\partial u_j}{\partial X_k} + \frac{\partial u_k}{\partial X_j}\right). \tag{3}$$

System of equations (1) is equipped with zero initial conditions and the following conditions

$$\begin{aligned} &\text{a)} && \mathbf{u}(X,t) = \mathbf{0}, && \text{for } X \in \Gamma^s_{\mathrm{Dir}}, \\ &\text{b)} && \tau^s_{ij}(X,t)\, n^s_j(X) = q^s_i(X,t), && \text{for } X \in \Gamma_{\mathrm{W_{ref}}}, \end{aligned} \tag{4}$$

where $n^s_j(X)$ are the components of the unit outer normal to $\Gamma_{\mathrm{W_{ref}}}$. The second equation is the Neumann boundary condition prescribing the action of the aerodynamic forces $\mathbf{q}^s = (q^s_1, q^s_2)$.

ALE method

The ALE method enables to treat the fluid domain changes. The ALE method is based on a diffeomorphism mapping A_t of the reference domain $\Omega^f_{\rm ref}$ onto the domain $\Omega^f_{\rm t}$ at any time instant $t \in (0, \mathrm{T})$, i.e. $x = A_t(X) \in \Omega^f_t$ for $X \in \Omega^f_{\rm ref}$. Assuming that $\frac{\partial A_t}{\partial t} \in C(\overline{\Omega^f_{\rm ref}})$ the ALE domain velocity $\mathbf{w}_D$ is defined by

$$\mathbf{w}_D(x,t) = \frac{\partial}{\partial t} A_t(X), \quad t \in (0,\mathrm{T}),\ X \in \Omega^f_{\rm ref}. \tag{5}$$

Further, the ALE derivative is introduced as the time derivative of an arbitrary continuous function $f(x,t) = f(A_t(X),t)$ with respect to a fixed point $X \in \Omega^f_{\rm ref}$, i.e.

$$\frac{D^A}{Dt} f(x,t) = \frac{d}{dt}\left(f(A_t(X),t)\right) = \frac{\partial f}{\partial t}(x,t) + \mathbf{w}_D(x,t)\cdot\nabla f(x,t), \tag{6}$$

where the chain rule was applied. For more details and for the proof see [53] or [23].

3.2 Fluid flow

The incompressible viscous fluid in $\Omega^f_{\rm t}$ is modelled by the the Navier-Stokes equations in the ALE form

$$\frac{D^A\mathbf{v}}{Dt} + ((\mathbf{v}-\mathbf{w}_D)\cdot\nabla)\mathbf{v} + \nabla p = \nu^f \Delta\mathbf{v} + \mathbf{g}^f, \quad \mathrm{div}\,\mathbf{v} = 0, \quad \text{in } \Omega^f_t, \tag{7}$$

where $\mathbf{v}(x,t)$ denotes the fluid velocity, p is the kinematic pressure and ν^f is the kinematic fluid viscosity, see e.g. [23].

Equations (7) are supplied by zero initial condition and these boundary conditions

$$\begin{aligned}
&\text{a)} && \mathbf{v}(x,t) = \mathbf{w}_D(x,t) && \text{for } x \in \Gamma_{\rm W_t} \cup \Gamma^f_{\rm Dir}, \qquad (8)\\
&\text{b)} && \text{c1)}\ \ \mathbf{v}(x,t)\cdot\mathbf{n}^f = 0, \quad \text{c2)}\ \ \frac{\partial(\mathbf{v}\cdot\mathbf{t}^f)}{\partial\mathbf{n}^f} = 0 && \text{for } x \in \Gamma^f_{\rm Sym},\\
&\text{c)} && (p(x,t) - p_{\rm ref})\mathbf{n}^f = \nu^f \frac{\partial\mathbf{v}}{\partial\mathbf{n}^f} - \frac{1}{2}\mathbf{v}(\mathbf{v}\cdot\mathbf{n}^f)^-, && \text{for } x \in \Gamma^f_{\rm Out},
\end{aligned}$$

for any $t \in (0,\mathrm{T})$. Vectors $\mathbf{n}^f$ and $\mathbf{t}^f$ are the unit outward normal and the unit tangent to boundary $\partial\Omega^f_{\rm t}$, respectively. Symbol $(\alpha)^-$ denotes $(\alpha)^- = \min(\alpha, 0)$, and $p_{\rm ref}$ is a reference pressure. Condition (8 d) is so called directional do-nothing boundary condition and it increases the stability of the model by suppressing possible backward flow through the outlet, see [19], [3].

At the inlet part of the boundary several possible forms of boundary conditions are considered. For this purpose the inlet boundary is formally divided into three disjoint parts: $\Gamma^f_{\rm In} = \Gamma^f_{\rm In,dir} \cup \Gamma^f_{\rm In,p} \cup \Gamma^f_{\rm In,\epsilon}$. The following boundary conditions are considered for any $t \in (0,\mathrm{T})$:

$$\begin{aligned}
&\text{a)} && \mathbf{v}(x,t) = \mathbf{v}_{\rm Dir}(x,t), && \text{for } x \in \Gamma^f_{\rm In,dir}, \qquad (9)\\
&\text{b)} && (p(x,t) - p_{\rm in})\mathbf{n}^f - \nu^f \frac{\partial\mathbf{v}}{\partial\mathbf{n}^f}(x,t) = -\frac{1}{2}\mathbf{v}(\mathbf{v}\cdot\mathbf{n}^f)^-, && \text{for } x \in \Gamma^f_{\rm In,p},\\
&\text{c)} && (p(x,t) - p_{\rm in})\mathbf{n}^f - \nu^f \frac{\partial\mathbf{v}}{\partial\mathbf{n}^f}(x,t) = -\frac{1}{2}\mathbf{v}(\mathbf{v}\cdot\mathbf{n}^f)^- + \frac{1}{\epsilon}(\mathbf{v}-\mathbf{v}_{\rm Dir}), && \text{for } x \in \Gamma^f_{\rm In,\epsilon}.
\end{aligned}$$

The choice of the inlet boundary condition is done e.g. by setting $\Gamma^f_{\rm In} = \Gamma^f_{\rm In,dir}$ and $\Gamma^f_{\rm In,p} = \Gamma^f_{\rm In,\epsilon} = \emptyset$. This notation facilitates the explanation of the weak formulation in the next chapter.

Condition (9 a) represents the classical Dirichlet boundary condition for velocity. Condition (9 b) can be understand as prescribing pressure difference $\Delta p = p_{\rm in} - p_{\rm ref}$ between the inlet $\Gamma^f_{\rm In}$ and the outlet $\Gamma^f_{\rm Out}$. Boundary condition (9 c) prescribes inlet airflow velocity $\mathbf{v}_{\rm Dir}$ by the penalization approach with the help of a suitable chosen penalization parameter ϵ, see [16], [52]. The value of parameter ϵ controls the switching between the Dirichlet boundary condition (limit $\epsilon \to 0^+$) and the pressure drop boundary condition (limit $\epsilon \to +\infty$).

Coupled FSI problem

The FSI problem is a coupled problem where the location of interface Γ_{W_t} is unknown and depends on established force equilibrium between the aerodynamic and the elastic forces.

Further, the structure and the fluid subproblems are coupled by the boundary conditions at interface $\Gamma_{\mathrm{W_t}}$. The BC for the fluid flow has the form of Dirichlet boundary condition (8 b). The BC for the elastic body is given by condition (4 b), where the vector $\mathbf{q}^s = (q_i^s)$ reads

$$q_i^s(X,t) = -\sum_{j=1}^{2} \sigma_{ij}^f(x,t)\, n_j^f(x), \qquad x = X + \mathbf{u}(X,t),\ X \in \Gamma_{\mathrm{W_{ref}}}, \tag{10}$$

where $\sigma_{ij}^f = -\rho^f p\, \delta_{ij} + \rho^f \nu^f (\frac{\partial v_i}{\partial x_j} + \frac{\partial v_j}{\partial x_i})$ are the components of fluid stress tensor.

3.3 Aeroacoustics

The acoustic domain Ω^a is shown in Figure 2. It is composed of two subdomains $\Omega^a_{\mathrm{prop}}, \Omega^a_{\mathrm{pml}}$. The domain of acoustic propagation Ω^a_{prop} consists of three parts $\Omega^a_{\mathrm{src}}, \Omega^a_{\mathrm{tract}}$ and Ω^a_{free}. Domain Ω^a_{src} is the domain, where the acoustic sources are evaluated from the flow simulation. Domain $\Omega^a_{\mathrm{tract}}$ represents the vocal tract and domain Ω^a_{free} models outer space (free field region). Finally, the perfectly matched layer (PML) domain Ω^a_{pml} encloses domain Ω^a_{free} in order to absorb outgoing sound waves.

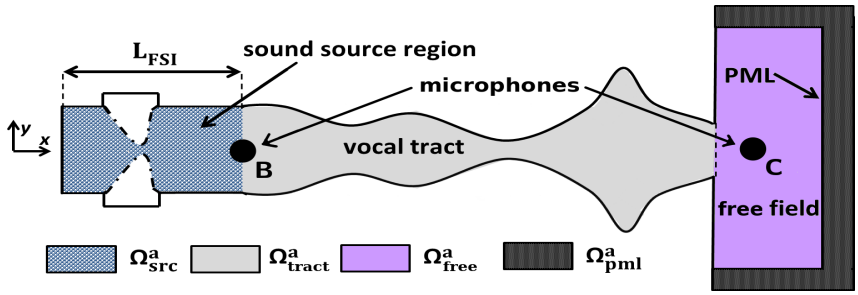

Figure 2: Scheme of acoustic domain. Propagation domain consists of the sound source region, the vocal tract and the free field. The propagation region is enclosed by the PML region.

Aeroacoustics is interested in aerodynamically produced sound in air, typically sound generated by a (turbulent) flow around obstacles, see e.g. [34], [30]. The flow-induced sound propagation can be described by the compressible Navier–Stokes equations (NSE). However, the acoustic part is only a very tiny component of the overall NSE solution, see e.g. [30], and thus it is very difficult to approximate it numerically. Thus the hybrid approach separating the description of the fluid flow and the acoustic problem is chosen here. It allows to use problem-specific numerical schemes on the other hand the hybrid approach neglects the acoustic influence on the flow field. In next paragraphs three different aeroacoustic approaches are presented.

Lighthill analogy

The Lighthill approach, see [37], reformulates the compressible NSE into an inhomogeneous wave equation

$$\left(\frac{1}{c_0^2}\frac{\partial^2}{\partial t^2} - \Delta\right) p' = \frac{\partial^2 T_{ij}}{\partial x_i \partial x_j}, \tag{11}$$

with notation of the pressure fluctuation p' and the speed of sound c_0. The sound sources are given by the divergence of the divergence of the Lighthill tensor $\mathbf{T} = (T_{ij})$ with components

$$T_{ij} = \rho v_i v_j + \left(p' - c_0^2 \rho'\right) \delta_{ij} - \tau_{ij}^f, \tag{12}$$

see e.g. [37], [30]. Let us emphasize that equation (11) is nonlinear as Lighthill tensor $\mathbf{T}$ depends on the pressure p'. For low Mach number flows usually the approximation, see [37],

$$T_{ij} \approx \rho_0 v_i v_j \tag{13}$$

is used. Then the formulation of Lighthill analogy (11) with (13) is already linear problem.

In this approach pressure fluctuation p' is not equal to acoustic pressure p^a but it must be regarded as a superposition of the acoustic and the hydrodynamic pressure, see [30].

Hybrid methods based on perturbation equations

Here, the perturbed convective wave equation (PCWE) and the aeroacoustic wave equation (AWE) approaches are presented, which are based on the acoustic/hydrodynamic splitting of the flow variables as introduced in work of [31]. The splitting is motivated by three properties of the acoustic field: a) it is fluctuating, b) it is irrotational and c) the acoustic pressure p^a does not coincide in general with pressure fluctuations p', see [48]. This splitting reads

$$\mathbf{v} = \overline{\mathbf{v}} + \mathbf{v}^{\mathrm{v}}(t) + \mathbf{v}^a(t), \quad p = \overline{p} + p^{\mathrm{v}}(t) + p^a(t), \quad \rho = \overline{\rho} + \rho^1(t) + \rho^a(t), \tag{14}$$

where $\mathbf{v}^{\mathrm{v}}, p^{\mathrm{v}}$ denote vortical fluctuating components and $\mathbf{v}^a, p^a, \rho^a$ are compressible (acoustic) fluctuations, see [44].

The perturbation equations for acoustic velocity $\mathbf{v}^a$ and acoustic pressure p^a for low Mach number regime is given by following set of equations, see [31],

$$\frac{\partial \mathbf{v}^a}{\partial t} + \nabla(\overline{\mathbf{v}} \cdot \mathbf{v}^a) + \frac{1}{\overline{\rho}} \nabla p^a = 0, \qquad \frac{\partial p^a}{\partial t} + c_0^2 \rho_0 (\nabla \cdot \mathbf{v}^a) + \overline{\mathbf{v}} \cdot \nabla p^a = -\frac{\partial p^{ic}}{\partial t} - \overline{\mathbf{v}} \cdot \nabla p^{ic}, \tag{15}$$

where the notation for incompressible quantities is introduced as $\mathbf{v}^{\mathrm{ic}} = \overline{\mathbf{v}} + \mathbf{v}^{\mathrm{v}}$, $p^{\mathrm{ic}} = \overline{p} + p^{\mathrm{v}}$.

PCWE. The formulation given by equations (15) can be rewritten with the help of the substantial derivative $\frac{D}{Dt} = \frac{\partial}{\partial t} + \overline{\mathbf{v}} \cdot \nabla$ and the introduction of the acoustic potential ψ^a. The PCWE approach reads, see [44],

$$\frac{1}{c_0^2} \frac{D^2 \psi^a}{Dt^2} - \Delta \psi^a = -\frac{1}{\rho_0 c_0^2} \frac{D p^{\mathrm{ic}}}{Dt}. \tag{16}$$

In numerical simulations we further simplify PCWE equation by disregarding the convection effects on the left-hand side of equation (16), i.e. $\frac{D^2\psi^a}{Dt^2}$ is replaced by $\frac{\partial^2 \psi^a}{\partial t^2}$, while keeping the full version of the right hand side in order to capture all sound sources, see [2].

AWE. AWE formulation is another simplification of (15) neglecting small convection effects. It reads, see [44],

$$\frac{1}{c_0^2} \frac{\partial^2 p^a}{\partial t^2} - \Delta p^a = -\frac{1}{c_0^2} \frac{\partial^2 p^{\mathrm{ic}}}{\partial t^2}. \tag{17}$$

The (aero-)acoustic problems are equipped by the **sound hard boundary condition** at $\partial\Omega^a$. The simulation of an open-boundary around free field domain is practically realized by the PML technique. The **PML** consists of a few additional layers of elements with artificial damping of the sound waves. The most important property is that there is no reflection at the interface between the propagation domain and the PML domain, see e.g. [34].

Coupled FSAI problems

In the FSAI problem the acoustic field is coupled with the FSI problem by the structure-acoustic and by the flow-acoustic couplings.

Structure-acoustic coupling. The vibroacoustic problem is given by coupling of elasticity equations (1) and the homogenous wave equation through boundary conditions. The BC prescribed to the acoustic problem is, see [34],

$$\frac{\partial p^{\mathrm{va}}}{\partial \mathbf{n}^a}(x,t) = -\rho^f \frac{\partial^2 \mathbf{u}}{\partial t^2} \cdot \mathbf{n}^a, \qquad x \in \Gamma_{\mathrm{W_{ref}}},\ t \in (0, \mathrm{T}). \tag{18}$$

For the elastic problem the coupling condition is neglected due to very tiny magnitude of p^{va}.

Flow-acoustic coupling If the aeroacoustic problem is modelled by hybrid methods, acoustics and the fluid flow problem are solved separately. Sound sources from fluid flow are computed and used in acoustics (as a volume coupling) whereas acoustic influence on fluid flow is omitted.

4 Numerical model

This section contains a detailed description of numerical schemes based on the finite element method applied for approximation of all three FSAI subproblems. For the purpose of time discretization the equidistant division of the time interval is used with the same time step Δt, i.e. the time interval $[0, \mathrm{T}]$ is divided into intervals given by the partition $t_n = n\Delta t$ for $n = 0, 1, \ldots, N$.

4.1 Elastic body

To achieve weak formulation, equation (1) is multiplied by a test function $\boldsymbol{\psi} = (\psi^1, \psi^2)$ from space $\mathbf{V} = \{\mathbf{f} \in \mathbf{H}^1(\Omega^s) | \mathbf{f} = 0 \text{ on } \Gamma^s_{\mathrm{Dir}}\} \subset \mathbf{H}^1(\Omega^s)$ and integrated over Ω^s. The application of the Green theorem and Hooke law (2) leads to the form

$$\left(\rho^s \frac{\partial^2 u_i}{\partial t^2}, \psi^i\right)_{\Omega^s} + \left(\left(\lambda^s \delta_{ij} \left(\operatorname{div} \mathbf{u}\right) + 2\mu^s e^s_{ij}(\mathbf{u})\right), e^s_{ij}(\boldsymbol{\psi})\right)_{\Omega^s} = \left(f^s_i, \psi^i\right)_{\Omega^s} + \left(q^s_i, \psi^i\right)_{\Gamma_{\mathrm{W_{ref}}}}, \quad (19)$$

where by symbol $(\cdot, \cdot)_{\mathcal{D}}$ the scalar product in space $L^2(\mathcal{D})$ is denoted.

The approximate solution $\mathbf{u}_h$ is sought in a finite dimensional finite element space $\mathbf{V}_h \subset \mathbf{V}$ with $2N_h$ basis functions $\boldsymbol{\psi}_j$. Then the approximate solution $\mathbf{u}_h$ at time $t \in (0, \mathrm{T})$ can be written as $\mathbf{u}_h(X, t) = \sum_{j=1}^{2N_h} \alpha_j(t)\, \boldsymbol{\psi}_j(X)$, where we further assume that unknown coefficients of the linear combination are $\alpha_j(t) \in C^2([0, \mathrm{T}])$.

This expression for $\mathbf{u}_h$ leads to the system of $2N_h$ ordinary differential equations of the second order for the unknown vector of coefficients $\boldsymbol{\alpha}(t) = (\alpha_j(t))_{j=1}^{2N_h}$

$$\mathbb{M}\ddot{\boldsymbol{\alpha}} + \mathbb{D}\dot{\boldsymbol{\alpha}} + \mathbb{K}\boldsymbol{\alpha} = \mathbf{b}(t), \quad (20)$$

where the term $\mathbb{D}\dot{\boldsymbol{\alpha}}$ was added with the matrix $\mathbb{D} = \epsilon^s_1 \mathbb{M} + \epsilon^s_2 \mathbb{K}$ representing the proportional damping model with suitably chosen parameters $\epsilon^s_1, \epsilon^s_2$, see e.g. [23]. The vector $\mathbf{b} = \mathbf{b}(t)$ has the components $b_i = (\mathbf{f}^s, \boldsymbol{\psi}_i)_{\Omega^s} + (\mathbf{q}^s, \boldsymbol{\psi}_i)_{\Gamma_{\mathrm{W_{ref}}}}$.
The time discretization of semi-discrete problem (20) is realized by the Newmark method, see e.g. [34]. The Lagrange finite elements of the first order are utilized.

4.2 Fluid flow

The time discretization is for the fluid flow problem applied before the spatial discretization. Let us denote the approximations at the n-th time level by $\mathbf{v}^n \approx \mathbf{v}(t_n), p^n \approx p(t_n)$, etc. The ALE derivative is approximated with the backward difference formula of second order (BDF2) as

$$\frac{D^A \mathbf{v}}{Dt}(t_{n+1}) \approx \frac{3\mathbf{v}^{n+1} - 4\overline{\mathbf{v}}^n + \overline{\mathbf{v}}^{n-1}}{2\Delta t}, \quad (21)$$

where for a fixed time instant t_{n+1} we denote $\overline{\mathbf{v}}^i(x) = \mathbf{v}^i(\tilde{x})$ for $\tilde{x} = A_{t_i}(A^{-1}_{t_{n+1}}(x))$, $i \in \{n-1, n\}$ and $x \in \Omega^f_{t_{n+1}}$. Further, for the sake of simplicity we focus on the discretization at a fixed time instant t_{n+1} and thus in next sections we omit the index $n+1$, i.e. we denote $\mathbf{v} := \mathbf{v}^{n+1}, \Omega^f := \Omega^f_{t_{n+1}}$, etc.

In order to obtain the weak formulation of fluid flow problem (7) in space, the first and the second equation of (7) are multiplied by test functions $\boldsymbol{\varphi} \in \mathbf{X}$ and $q \in M$, respectively. Here the space $\mathbf{X} = X_1 \times X_2$ is defined as $X_1 = \{f \in H^1(\Omega^f) |\, f = 0 \text{ on } \Gamma^f_{\mathrm{Dir}} \cup \Gamma^f_{\mathrm{In,dir}} \cup \Gamma^f_{\mathrm{W_t}}\} \subset H^1(\Omega^f)$, $X_2 = \{f \in X_1 |\, f = 0 \text{ on } \Gamma^f_{\mathrm{Sym}}\}$ and $M = L^2(\Omega^f)$. Then both equations (7) are integrated over the fluid domain Ω^f, summed up into a single equation and the Green's theorem is multiple

times applied. The final weak formulation of problem (7) at time t_{n+1} can be written as: Find a such function pair $V = (\mathbf{v}, p) \in \mathbf{H}^1(\Omega^f) \times M$, that

$$a(V, V, \Phi) = f(\Phi) \tag{22}$$

is satisfied for any test function pair $\Phi = (\boldsymbol{\varphi}, q)$ from space $\mathbf{X} \times M$ and moreover velocity $\mathbf{v}$ satisfies boundary conditions (8 a, b, c1) and (9 a) and $\frac{D^A\mathbf{v}}{Dt} \in L^2(\Omega^f)$. The trilinear form $a(\cdot,\cdot,\cdot)$ with arguments $V^* = (\mathbf{v}^*, p^*), V = (\mathbf{v}, p)$ and $\Phi = (\boldsymbol{\varphi}, q)$ is given as

$$\begin{aligned} a(V^*, V, \Phi) = &\left(\frac{3\mathbf{v}}{2\Delta t}, \boldsymbol{\varphi}\right)_{\Omega^f} + \frac{1}{2}(((\mathbf{v}^* - 2\mathbf{w}_D)\cdot\nabla)\mathbf{v}, \boldsymbol{\varphi})_{\Omega^f} - \frac{1}{2}((\mathbf{v}^*\cdot\nabla)\boldsymbol{\varphi}, \mathbf{v})_{\Omega^f} + \\ &+ \frac{1}{2}((\mathbf{v}^*\cdot\mathbf{n})^+\mathbf{v}, \boldsymbol{\varphi})_{\Gamma^f_{\mathrm{Out}}} + \nu^f(\nabla\mathbf{v}, \nabla\boldsymbol{\varphi})_{\Omega^f} - (p, \operatorname{div}\boldsymbol{\varphi})_{\Omega^f} + (q, \operatorname{div}\mathbf{v})_{\Omega^f} + \\ &+ \frac{1}{2}((\mathbf{v}^*\cdot\mathbf{n})^+\mathbf{v}, \boldsymbol{\varphi})_{\Gamma^f_{\mathrm{In,p}}} + \frac{1}{2}((\mathbf{v}^*\cdot\mathbf{n})^+\mathbf{v}, \boldsymbol{\varphi})_{\Gamma^f_{\mathrm{In},\epsilon}} + \frac{1}{\epsilon}(\mathbf{v}, \boldsymbol{\varphi})_{\Gamma^f_{\mathrm{In},\epsilon}}, \end{aligned} \tag{23}$$

where the formulation of convective term is motivated by the directional do-nothing BC (8 d) and the realization of penalization condition (9 c) leads to the last two terms of (23). The linear functional $f(\cdot)$ reads

$$f(\Phi) = \left(\frac{4\overline{\mathbf{v}}^n - \overline{\mathbf{v}}^{n-1}}{2\Delta t}, \boldsymbol{\varphi}\right)_{\Omega^f} + (p_{\mathrm{ref}}\mathbf{n}^f, \boldsymbol{\varphi})_{\Gamma^f_{\mathrm{Out}}} + \left(p_{\mathrm{in}}\,\mathbf{n}^f, \boldsymbol{\varphi}\right)_{\Gamma^f_{\mathrm{In,p}}} + \frac{1}{\epsilon}(\mathbf{v}_{Dir}, \boldsymbol{\varphi})_{\Gamma^f_{\mathrm{In},\epsilon}}. \tag{24}$$

Let us recall that in practice only one of the sets $\Gamma^f_{\mathrm{In,dir}}, \Gamma^f_{\mathrm{In,p}}, \Gamma^f_{\mathrm{In},\epsilon}$ is chosen to be nonempty leading to significant reduction of boundary terms in (23) and (24).

Stabilization During discretization of the problem (22) the velocity and the pressure spaces are replaced by finite element subspaces $\mathbf{H}_h \subset \mathbf{H}^1(\Omega^f)$ and $\mathbf{X}_h = \mathbf{X} \cap \mathbf{H}_h$, $M_h \subset M$. In order to obtain stable method the finite element spaces $\mathbf{X}_h, M_h$ have to fulfill the Babuška–Brezzi condition *inf-sup condition*, see e.g. [26]. For practical computation the chosen P1-bubble/P1 finite elements satisfy this condition, see [26].

Nevertheless, the FE solution can be numerically unstable in the case of high Reynolds number flows, when the convection dominates. This is principally caused by the unresolved velocity gradients due to too coarse grid. In order to overcome the possible numerical instability a combination of the streamline-upwind/Petrov-Galerkin method (SUPG) and pressure-stabilization method (PSPG) together with *div-div* stabilization are applied, see e.g. [25], [23]. The nonlinear system of equations (22) is linearized with the aid of fixed point iterations.

4.3 FSI coupling

This paragraph presents two ingredients of FSI numerical solution – the construction of ALE mapping and the way how is the aerodynamic forces computed.

Construction of ALE mapping. The ALE mapping A_t should provide smooth mapping Ω^f_{ref} onto Ω^f_{t} for any $t \in (0, \mathrm{T})$, which is quite robust, easy to implement and capable to handle very complex domain deformation. These requirements are fulfilled by the pseudo-elastic approach, see e.g. [38]. The pseudo-elastic approach seeks the solution of an artificial stationary elasticity problem on Ω^f_{ref} with known deformation of the boundary $\partial\Omega^f_{\mathrm{ref}}$, see [4].

Dynamic coupling condition In order to take into account also the dynamic coupling condition of form (4 b) the aerodynamic forces acting on the structure needs to be evaluated. Here, three applicable methods of the aerodynamic forces evaluation are considered.

The first approach of the dynamic coupling condition evaluation is the **extrapolation** of the aerodynamic quantities from the interior of the fluid domain onto boundary $\Gamma_{\mathrm{W_t}}$ and then use these extrapolated values to approximate aerodynamic forces $\mathbf{q}^s$ given by (10).

The second possibility is the application of the **local reconstruction technique** introduced by Babuška, see e.g. [15], which can possibly increase the accuracy of aerodynamic forces computation in comparison with the previous approach. The idea is based on the reconstruction of the velocity gradient at arbitrary vertex of fluid mesh $\mathcal{T}_h^f$ using the patch of neighbouring triangles and the least square method.

The third possibility how to calculate the aerodynamic forces is to use their **weak reformulation**. In this case boundary condition (4 b) is rather evaluated in the weak form $(\mathbf{q}^s, \boldsymbol{\varphi}_i)_{\Gamma_\mathrm{W}}$, see e.g. [24]. This results in replacement of the surface integral by the volume integrals and the reaching of the numerical accuracy of primal variables.

Solution of FSI coupled problem. For the solution of the FSI problem the strongly coupled partitioned algorithm is implemented. It means that the fluid flow and the structure subproblem is iteratively solved until the convergence test at the end of each cycle is passed, see e.g. [23] or [33].

4.4 Aeroacoustic problems

The aeroacoustic problem is given either by Lighthill analogy (11) or by simplified PCWE equation (16) or by AWE equation (17). In all cases the problem is described by the wave equation where only the sound source terms differ.

Lighthill analogy In order to derive weak formulation equation (11) is multiplied by a test function $\eta \in Y = H^1(\Omega^a_{\mathrm{prop}})$ and integrated over the propagation part of the acoustic domain Ω^a_{prop}. The application of the Green's theorem results in the following weak formulation for fixed time instant $t \in (0, \mathrm{T})$: Find a function $p' : (0, \mathrm{T}) \mapsto Y$ such, that

$$\left(\frac{1}{c_0^2}\frac{\partial^2 p'}{\partial t^2}, \eta\right)_{\Omega^a_{\mathrm{prop}}} + \left(\nabla p', \nabla \eta\right)_{\Omega^a_{\mathrm{prop}}} = -\left(\nabla \cdot (\rho_0 \mathbf{v} \otimes \mathbf{v}), \nabla \eta\right)_{\Omega^a_{\mathrm{src}}} \tag{25}$$

is satisfied for any test function $\eta \in Y$. It is moreover assumed that $\frac{\partial^2 p'}{\partial t^2} \in L^2(\Omega^a)$.
The solution $p' \in Y$ at time t is then approximated by p'_h using the finite element subspace Y_h of Y with the dimension N_h^a. It leads to the second order system of ODEs for the unknown vector $\boldsymbol{\gamma}^a(t) = (\gamma_j^a)$ in the form

$$\frac{1}{c_0^2}\mathbb{M}^a \ddot{\boldsymbol{\gamma}}^a + \mathbb{K}^a \boldsymbol{\gamma}^a = \mathbf{b}^a(t), \tag{26}$$

where $\mathbb{M}^a$ and $\mathbb{K}^a$ are the mass and the stiffness matrices, respectively. The vector $\mathbf{b}^a(t)$ is for the Lighthill analogy taken as $\mathbf{b}^a = \mathbf{b}^{LH} = (b_i^{LH})$, where

$$b_i^{LH}(t) = -\left(\rho_0 \frac{\partial (v_j v_l)}{\partial x_l}, \frac{\partial \eta_i}{\partial x_j}\right)_{\Omega^a_{\mathrm{src}}} \tag{27}$$

and the Einstein summing convection is applied, here specially for indices j and l.

For practical computation the quadratic Lagrange finite elements are chosen and system of ODEs (26) is numerically discretized in time by the Hilber-Hughes-Taylor-α (HHT-α) method, [34].

PCWE approach Here, the simplified version of PCWE approach (16) is considered. Using the same FE discretization procedure as for (25) we arrive to the system of ODEs (26), where the right hand side vector $\mathbf{b}^a(t)$ is now equal to $\mathbf{b}^{PCWE}(t)$ with the components b_i^{PCWE} computed according to

$$b_i^{PCWE} = -\left(\frac{1}{\rho_0 c_0^2}\left(\frac{\partial p^{ic}}{\partial t} + \overline{\mathbf{v}} \cdot \nabla p^{ic}\right), \eta_i\right)_{\Omega^a_{\mathrm{src}}}. \tag{28}$$

AWE approach The discretization of the AWE approach given by (17) is performed similarly as before, i.e. the FE discretization procedure for (25) results into system (26), where the right hand side vector $\mathbf{b}^a(t)$ is now replaced by $\mathbf{b}^{AWE}(t)$ with the components b_i^{AWE} given as

$$b_i^{AWE} = -\frac{1}{c_0^2}\left(\frac{\partial^2 p^{ic}}{\partial t^2}, \eta_i\right)_{\Omega^a_{\mathrm{src}}}. \tag{29}$$

Aeroacoustic source evaluation

Three numerical methods are described how the sound sources can be computed.

First, the LH sound sources (27) with the assumption of the incompressible flow can be simplified to

$$b_i^{LH} = \left(\rho_0 \frac{\partial v_l^{ic}}{\partial x_j}\frac{\partial v_j^{ic}}{\partial x_l}, \eta_i\right)_{\Omega^a_{\mathrm{src}}}. \tag{30}$$

An alternative approach how to evaluate formula (27) is based on FE weak reformulation effectively moving one spatial derivative from the computed airflow velocities to the test functions.

In the end, the local reconstruction can be applied on the velocity gradients e.g. in equation (30) or on the pressure gradient in (28).

Interpolation of sound sources. The sound sources evaluated on the CFD mesh primarily resolving thin boundary layers are interpolated on the acoustic mesh which is ideally uniform. The used interpolation procedure of the program CFS++ preserves the overall acoustic energy, see [34].

4.5 Vibroacoustics

Let us consider the vibroacoustic problem now. Due to omitted influence of the acoustics on the structure the coupled vibroacoustic problem simplifies to the acoustic problem with a given sound source at boundary $\Gamma_{\mathrm{W_{ref}}}$ given by BC (18) with the form of interface normal acceleration.

The weak formulation of the vibroacoustic problem reads: seek a such function $p^{\mathrm{va}} \in Y$ that

$$\left(\frac{1}{c_0^2}\frac{\partial^2 p^{\mathrm{va}}}{\partial t^2}, \eta\right)_{\Omega^a_{\mathrm{prop}}} + (\nabla p^{\mathrm{va}}, \nabla \eta)_{\Omega^a_{\mathrm{prop}}} = \left(\rho_0^f \frac{\partial^2 (\mathbf{u}\cdot\mathbf{n}^s)}{\partial t^2}, \eta\right)_{\Gamma_{\mathrm{W_{ref}}}} \tag{31}$$

is satisfied for any $\eta \in Y$. The application of the FE method leads to the system of ODEs (26), where the right hand side vector $\mathbf{b}^{\mathrm{va}}(t) = (b_i^{\mathrm{va}})$ is now given by

$$b_i^{\mathrm{va}} = \left(\rho_0^f \frac{\partial^2 (\mathbf{u}\cdot\mathbf{n}^s)}{\partial t^2}, \eta_i\right)_{\Gamma_{\mathrm{W_{ref}}}}. \tag{32}$$

4.6 Solution of FSAI coupled problem

The workflow of the FSAI algorithm consists of these steps:
1) Sound sources evaluation.
2) Sound sources interpolation on the (coarser) acoustic grid.
3) Solution of the sound propagation problem.

The vibroacoustic problem is in the FSAI problem omitted, it is analyzed in the separate study.

5 Numerical results of FSI problem

The numerical results consists of the FSI simulations first with a prescribed VF motion and second with apriori unknown VF motion. The different inlet boundary conditions are compared. Third, energy transfer between airflow and structure vibration is studied. The presented results are detailed version of publications [4, 7, 6, 10, 13].

The considered VF model and materials is taken from [52, 29] with assumed symmetry at axis $y = 0$ and the half-gap $g_0 = 0.4\,\mathrm{mm}$. The constant time step Δt is chosen as $2.5 \cdot 10^{-5}\,\mathrm{s}$.

Further, the static part of the aerodynamic force loading the elastic structure is eliminated from the dynamic response of the structure, i.e. the modified aerodynamic force $\mathbf{q}^s_{\mathrm{mod}}$ is prescribed by $\mathbf{q}^s_{\mathrm{mod}}(X,t) = \mathbf{q}^s(X,t) - \mathbf{q}^s_{\mathrm{stat}}(X)$, where static force $\mathbf{q}^s_{\mathrm{stat}}$ is computed in fixed channel configuration in the last time step before release of the structure for interaction.

5.1 Prescribed motion of structure

This section presents the results of numerical simulations for a prescribed motion of vocal folds, see [4]. In all cases the periodical motion of vocal fold is prescribed by

$$u_1(x,y,t) = 0, \qquad u_2(x,y,t) = \frac{C_{\mathrm{driven}}}{100} \cdot (y + g_0 + H_2) \cdot \sin(2\pi \cdot 100t), \tag{33}$$

where H_2 is the VF height, $C_{\mathrm{driven}} = 7.2$ is free parameter and half-gap $g_0 = 0.4\,\mathrm{mm}$ is fixed.

Effect of the inlet boundary conditions on flow characteristics. The performance of considered boundary conditions (9) is tested for the case of prescribed VF motion of form (33) which enables nearly full closing of the channel up to the minimal half-gap $g_{0,min} = 0.0114\,\mathrm{mm}$. Further, three inlet boundary conditions are considered:

1) Dirichlet boundary condition (9 a) with the given inlet velocity referred as "vel",

2) the case with the prescribed pressure drop by condition (9 b) labeled as "pres",

3) the case of penalization boundary condition (9 c) denoted as "pen".

The inlet velocity and the pressure drop are set as $\mathbf{v}_{\mathrm{Dir}} = (1.7, 0)\,\mathrm{m/s}$ and $\Delta p = 400\,\mathrm{Pa}$, respectively. The penalization parameter is chosen as $\epsilon = 5 \cdot 10^{-4}\,\mathrm{s/m}$.

The different behaviour of the inlet flow velocity and the pressure drop in all three studied cases is shown in Figure 3. The inlet velocity is constant for the case "vel" and oscillating for the case "pres" around its mean value (approximately the same as for "vel"). In the case "pen" the inlet velocity for the open channel is the same as for case "vel", but during the channel closing drops rapidly near to zero. On the other hand, the pressure drop in the case "pres" is almost constant, while for the case "vel" the pressure grows fast to unphysically high albeit expected values during the channel closing. In the case "pen" the pressure drop remains bounded with reasonable amplitude comparable with experiments, see [27]. The maximal value of the pressure drop is therein after referenced as the pressure peak.

Parametric study of an optimal value of the penalty parameter. The dependence of the (maximal) pressure drop on the penalization parameter ϵ is shown in Figure 4, which presents also the dependence of the maximal, the average and the minimal flow rate Q on the parameter ϵ. The maximal and the minimal flow rate means the maximal and the minimal instant value over the whole simulation time. The most rapid changes occur for the penalization parameter in the range $10^{-7} - 10^{-4}\,\mathrm{s/m}$, where the pressure peaks demonstrate a steep decrease from its maximum (circa $500\,\mathrm{kPa}$) close to minimal values ($< 20\,\mathrm{kPa}$) and the average flow rate is still close to its maximum.

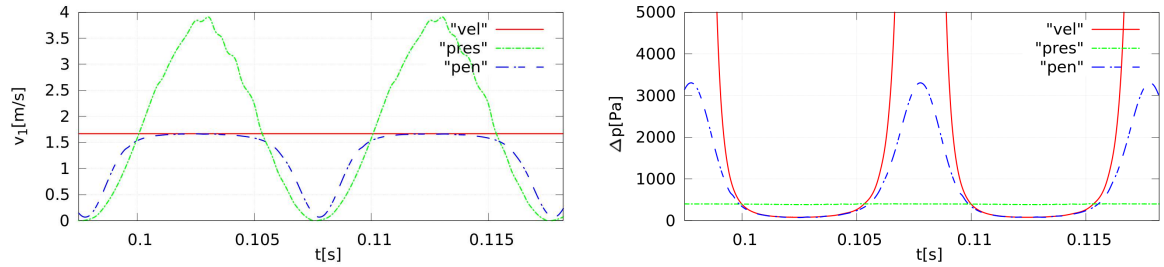

Figure 3: **Left:** The inlet velocity (averaged over Γ_{In}^{f}) in the dependence on time. **Right:** The pressure drop during two periods of the reference prescribed motion. The pressure drop in the case of "vel" has unrealistic high maximum of circa 472 kPa.

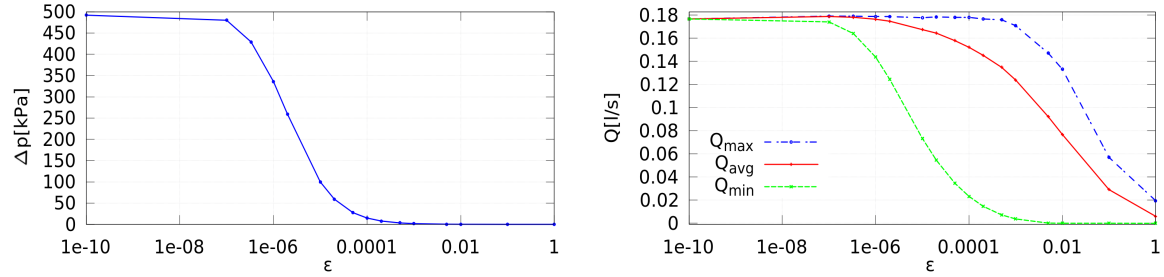

Figure 4: The dependence of the maximal pressure drop and the inlet flow rate on the penalization parameter ϵ is plotted at the top and at the bottom, respectively.

The graphs shown in Figure 4 allow to estimate the suitable value of the penalization parameter according to measured pressure drop and flow rate values. For the simulation of flow-induced VF vibrations the typical range of transglottal pressures and flow rates are approximately $0.1 - 2.0\,\mathrm{kPa}$ and $0.05 - 0.5\,\mathrm{l/s}$, resp., see [56]. For the current setting is reasonable to choose the penalization parameter in range $2 \cdot 10^{-4} < \epsilon < 5 \cdot 10^{-3}$.

Choice of the parameters according to experimental data. Here we show the dependence of the pressure drop on the gap area during one regular VF oscillation cycle as it was measured in laboratory experiment, see [28]. This dependence allows to estimate the transferred energy from airflow to the VF vibration E_{transf}. Figure 5 (left) shows the accumulated energy in the case of self-induced vibration of VFs as measured by [28] on the VF model with included the vocal tract model and driven by constant flow rate $Q = 0.2\,\mathrm{l/s}$. The accumulated energy is in this case positive due to clockwise orientation of the pressure-gap area curve.

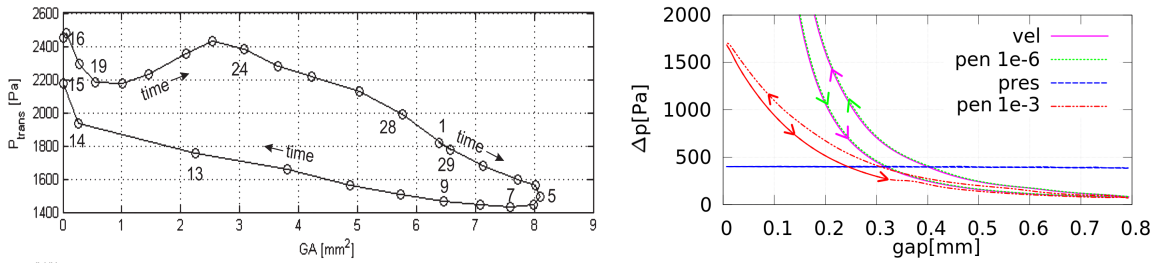

Figure 5: **Right:** Typical behaviour of the transglottal pressure in the dependence on the glottal gap area (GA) during one oscillation cycle, [28]. **Left:** Dependence of the transglottal pressure on the gap for four simulation cases.

The pressure-gap dependence constructed using the previously presented FSI simulations is shown in Figure 5 (right). As expected, in the case "vel" the pressure maximum is unrealistically high. The same behaviour can be observed for the penalization approach with $\epsilon = 10^{-6}$ s/m. For the case "pres" the pressure drop remains almost constant. Finally choice of the penalization approach with $\epsilon = 10^{-3}$ s/m demonstrates the qualitative agreement with results published in [28] in terms of maximal pressure. The sum of transferred energy is negative in all cases due to an anticlockwise curve orientation what is typical for the prescribed motion of VF. The conclusions of this qualitative comparison have to be done very carefully because the numerical gap-pressure dependence is obtained in highly different configurations.

5.2 Fluid-structure interaction of the hemi-larynx configuration

This paragraph contains the comparison of the flow inlet BC for full FSI problem and the sensitivity of the flutter airflow velocity on the penalization parameter ϵ.

Influence of the inlet boundary conditions on the flow-induced vibrations Similarly as in the previous section the influence of inlet boundary conditions (9) is here studied on the examples of four numerical simulations. The inlet velocity $v_{\mathrm{Dir},1} = 1.9\,\mathrm{m/s}$ is prescribed by condition (9 a) (case "Vel") and by (9 c) with two different choices of penalization parameter $\epsilon = 10^{-5}\,\mathrm{s/m}$ and $\epsilon = 5 \cdot 10^{-4}\,\mathrm{s/m}$. These two cases are denoted as "Pen-S" (strong) and "Pen-W" (weak) case, respectively. The case of the applied condition (9 b) is labeled as "Pres"with chosen pressure drop $\Delta p = p_{\mathrm{in}} - 0 = 450\,\mathrm{Pa}$.

The computed pressure drop and the half-gap $g_0(t)$ are displayed in Figure 6. The pressure drop in case "Pres" is almost constant while for the prescribed inlet velocity in cases "Vel", "Pen-S" and "Pen-W" the pressure drop shows significant oscillating behaviour connected with the increasing VFs vibration amplitude monitored in Figure 6 right. In the case of penalization approach the pressure drop oscillation is delayed.

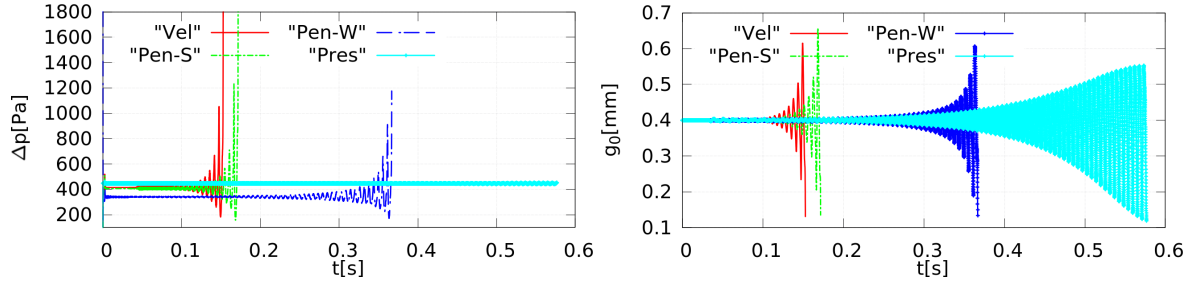

Figure 6: **Left:** Pressure drop between the inlet and the outlet. **Right:** Time development of the half-gap plotted for cases "Vel", "Pen-S", "Pen-W" and "Pres".

Neither boundary condition (9 a) nor boundary condition (9 c) corresponds to reality because both the inlet flow velocity and the inlet pressure should fluctuate as it was observed e.g. in the measurements [27]. This behaviour is recovered using the penalization approach. In all four cases the inlet flow velocity exceeds the critical flutter velocity $v_{\mathrm{flutter}} \approx 1.86\,\mathrm{m/s}$, see [7].

Determining the boundary of the flutter instability The dependence of critical velocity v_{flutter} on the penalization parameter ϵ is investigated and summarized in Figure 7. The influence of penalization parameter is proven to be negligible for values $\epsilon < 10^{-4}$, while for $\epsilon > 10^{-4}$ the influence is quickly increasing, see [7]. Therefore we recommend to restrict the suitable range of penalization parameter ϵ for the simulation of flow-induced VF vibrations to range $2 \cdot 10^{-4} < \epsilon < 1 \cdot 10^{-3}$, i.e. $\frac{1}{5000} < \epsilon < \frac{1}{1000}$.

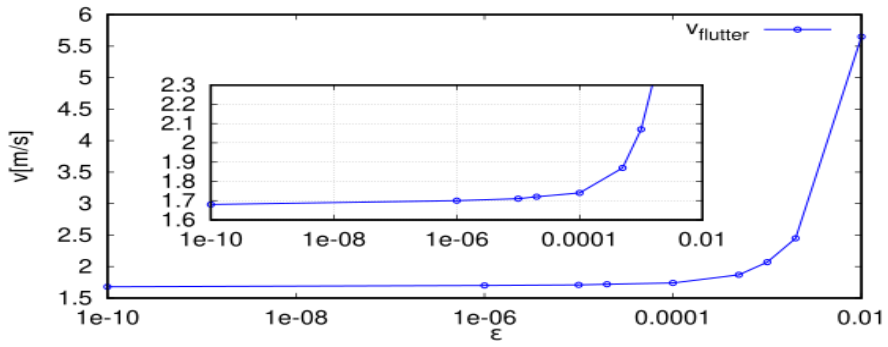

Figure 7: Dependence of the critical flutter velocity for the hemi-larynx configuration on the penalization parameter.

5.3 Energetic considerations related to the VF flutter

Flutter phenomenon of the FSI system can in general emerge and can be maintained if the total energy gained from airflow by structure exceeds the energy loss caused by the structure damping and the damping due to the fluid viscosity. A positive flow of energy from the airstream to the structure tissue occurs if the aerodynamic (VF driving) force is in phase with the tissue velocity, see [55]. Here, the energy exchange between vibrating VF and fluid flow is quantified based on the previous numerical simulations, see also [10].

The rate of energy transfer (power) $\dot{E}_{transf}$ at time instant t done by fluid stress on the (structure) surface is given by, see [54],

$$\dot{E}_{transf} = \int_{\Gamma_{W_t}} v_i \, \sigma_{ij}^f \, (-n_j^f) \, dS = \int_{\Gamma_{W_t}} \frac{\partial u_i}{\partial t} \, \sigma_{ij}^f \, n_j^s \, dS, \tag{34}$$

where the equality $\mathbf{v} = \frac{\partial \mathbf{u}}{\partial t}$ and $\mathbf{n}^f = -\mathbf{n}^s$ at Γ_{W_t} is used. The cumulative transferred energy (work) during a certain time interval can be calculated as $E_{cumul}(t) = \int_0^t \dot{E}_{transf}(\tau) \, \mathrm{d}\tau$.

The computed functions $\dot{E}_{transf}$ and E_{cumul} are shown in Figure 8 for the previously presented numerical results of full FSI problem and simulation with the prescribed VF motion earlier labeled “pen” and here referred as “Driven”.

In all full FSI cases the energy transfer function oscillates around zero with growing amplitude, see Figure 8. The function $\dot{E}_{transf}$ develops in time the most intensively for case “Vel” followed by case “Pen-S”, in case “Pres” the oscillation magnitude of function $\dot{E}_{transf}$ grows slowly. The function E_{cumul} practically copies the behaviour of $\dot{E}_{transf}$ with an exponentially increasing average value, around which it oscillates. It is expected behaviour, because the prescribed inlet velocity (or the pressure drop) is higher than the critical flutter velocity, see [51]), and the energy growth confirms previously observed flutter instability. In case “Driven” the function E_{cumul} is linearly decreasing, see Figure 8, as it was already noticed in paragraph 5.1.

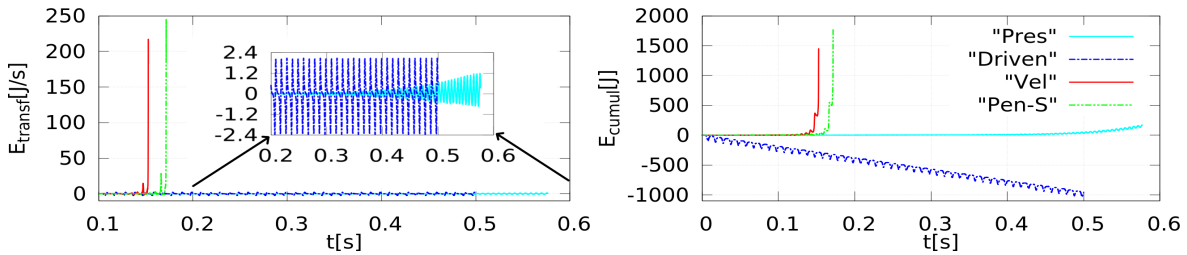

Figure 8: Energy transfer function (left) and energy cumulative function (right) for cases “Vel”, “Pen-S”, “Pres” and “Driven”.

6 Numerical results of FSAI problem

This section presents the numerical results of aero- and vibro-acoustic problems. These results are based on the results of FSI simulation. The acoustic computations start with the determination of the resonant frequencies of the vocal tract models.

FSI numerical results

The used vocal fold model is based on the VF shape and material parameters published in article [61], see also publication [2]. The initial (full) glottal gap equal to 2.0 mm, the pressure drop $\Delta p = p_{\text{in}} - 0 = 1500\,\text{Pa}$ is prescribed and the constant time step $\Delta t = 2.5 \cdot 10^{-5}\,\text{s}$ is chosen.

Figure 9 illustrates a typical behaviour of flow-induced vibration at selected point A from the top surface of VF. The spectrum of VF displacement shows two dominant frequencies $f_1 = 121$ and $f_2 = 211$ Hz. The frequencies f_1 and f_2 agree relatively well with the first two VF eigenfrequencies what is in good correspondence with the results of [61]. A typical picture of FSI solution is shown in Figure 10. Similar character of the complex flow field was reported in [33].

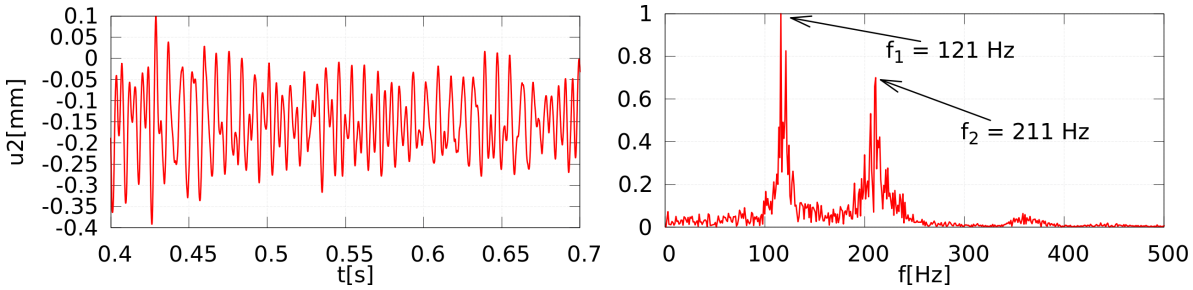

Figure 9: **Left:** Time evolution of the displacement of the chosen point A in y-direction. **Right:** Normalized Fourier transform of the time signal from the left.

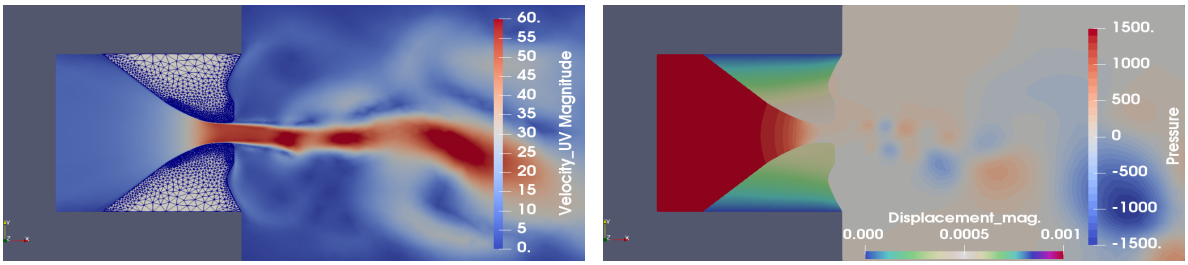

Figure 10: Typical picture of the airflow velocity distribution (left) and pressure and vocal fold displacement in mm (right).

6.1 Vocal tract resonances

The VT geometry co-determines the characteristics of propagated sound, where the VT resonances have one of the most important influences. That is why the several VT models are analyzed in order to find their acoustic resonant frequencies, in the human phonation context usually called formants, see [56]. The results are based on the publication [9].

The part of acoustic domain Ω^a_{tract} representing a VT model for the vowel [u:] is based on the data of acquired by MRI measurements [49]. Here due to 2D computations the (1D) diameters r_i of the VT model cross-sections are determined as the radius of published 2D cross-sections. The VT model of the vowel [u:] described now by 46 cross-section radii has the total length of $L \doteq 17.86\,\text{cm}$.

The modifications of the VT model are performed with the goal to quantify an influence of additional acoustic volume represented by the domain Ω^a_{src} and the prolongation region, which are (artificially) included for the reason of inclusion the CFD domain with the sound sources. Three variants of acoustic domain Ω^a geometry are considered, see Figure 11.

Transfer function approach and results The (inhomogeneous) wave equation transformed into frequency domain is called Helmholtz equation, see [30], and it reads

$$-\left(\frac{\omega^2}{c_0^2} + \Delta\right)\hat{p} = \hat{F}, \tag{35}$$

where ω denotes the angular frequency and the variables with caret ($\hat{p}$) denote the Fourier transforms of variables without caret (p). Assuming a unit harmonic excitation given by right hand sources $\hat{F}(\omega)$ at a given frequency ω let us seek for the system answer at the same frequency. The problem (35) is equipped with the sound hard BC at $\partial\Omega^a$ and the PML layer is applied on the boundary of the free field region in order to model the open boundary. The transfer function $H(\omega)$ denotes here the ratio of the amplitude of the (complex) acoustic pressure $\hat{p}$ monitored at a position x_M to the harmonic acoustic forcing $\hat{F}$ at a chosen excitation location Γ_{exc}. The evaluation of the transfer function $H(\omega)$ over a frequency interval provides us the resonant frequencies.

Problem (35) is numerically solved in the frequency range $50 - 3000$ Hz with logarithmic sampling, i.e. $f_{i+1} = q \cdot f_i$, by the solver CFS++ . The transfer functions computed for three vocal tract models M1, M2 and M4 are shown in Figure 11 (right) and they are compared with the first three formants of vowel [u:] from paper [49].

The behaviour of transfer functions for both models M1 and M2 is very similar, both show four formants in the range $50 - 2500$ Hz. A closer match to the measured formants has the VT model M2 than the model M1. The occurrence of third formant F3 at frequency 1432 Hz contrary to results of [49] could be probably caused by the longer acoustic domain (M1 is $\approx 23\,\text{cm}$ long). Finally model M4, the 2D version of published 3D VT shape, exhibits an acceptable match of the first three reference formants. Nevertheless, it should be mentioned that the comparison to the results of article [49] measured in humans during MRI examination is only indicative due to multiple reasons.

6.2 Vibroacoustic simulation

In this section the sound propagation is simulated, where the aeroacoustic sources are omitted and just the sound emitted by the vibrating VF as obtained by the FSI simulation is taken into account. Although the sound of vibroacoustic origin is usually considered to be small, see [59], recent thesis [39] showed that the acoustic emission could be significant. The presented results are an extended version of results published in [14] and [5].

The acoustic problem is solved within the vocal tract model M1. The virtual microphone C is placed approximately 2 cm in front of the (virtual) mouth. The sound induced by VF vibration is quite silent with SPL of circa 30 dB, see Figure 12. The first two VF eigenfrequencies are again the very dominant frequencies, similarly as in [39]. Further the first two formants also strongly

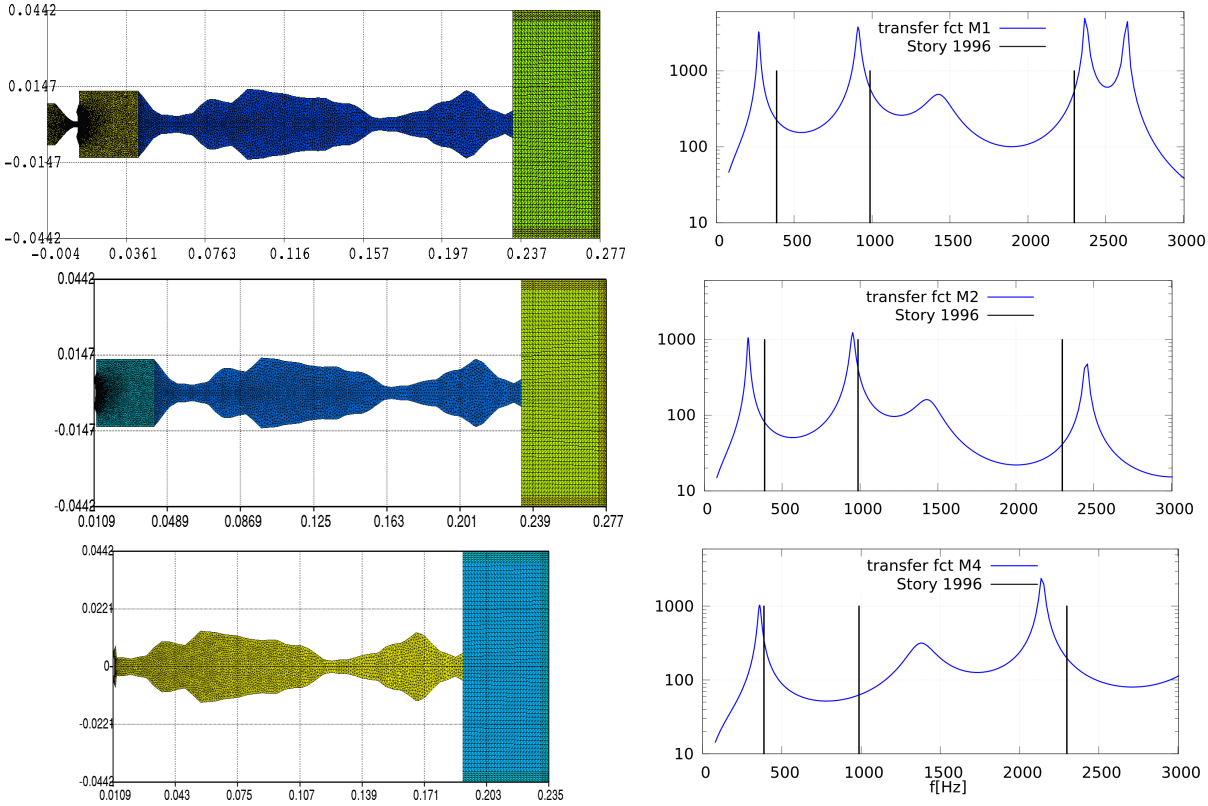

Figure 11: **Left:** Vocal tract acoustic models for cases M1, M2 and M4. **Right:** Graph of the computed transfer functions for given cases. The formants of the vowel [u:] are highlighted by black vertical lines located at $389, 987, 2299$ Hz (data from [49]).

represented in Figure 12, while the further M1 formants are less significant. The presented results show that the vibration-borne sound in the considered case without the VFs contact does not significantly contribute to the overall radiated SPL, see e.g. [60].

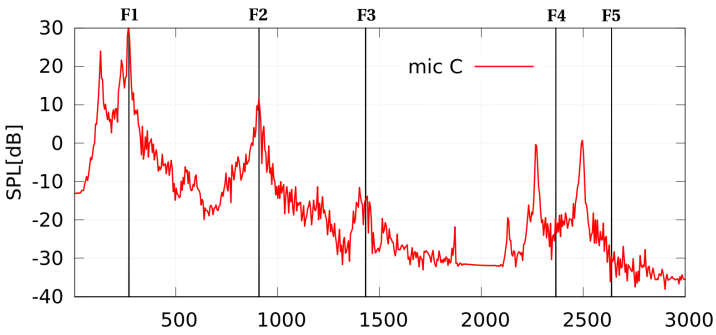

Figure 12: Sound pressure level in frequency domain computed at point C. The black vertical lines demonstrate first five formants of vocal tract model M1.

6.3 Aeroacoustic simulation

This section contains the sound sources analysis as they are calculated based on the numerical results of FSI problem. Then the simulation of the sound propagation through the VT model for the LH analogy, the (simplified) PCWE and the AWE approach is described. The presented

results are based on author's paper [2] and other published results [11, 8, 12].

Sound sources

The different numerical formulation of the LH sound sources is analyzed and the sound sources structure of three different modelling approaches are compared. Then their frequency content is investigated.

First, the LH sound sources are obtained by four different techniques, namely formula (30) is evaluated with and without the gradient reconstruction technique or by using the framework of radial basis functions (RBF), see [45], as the default option of the program CFSDat. The fourth possibility presents reformulation by the pressure Laplacian, see [34]. The LH sound sources obtained with and without the gradient reconstruction technique are very similar. The RBF approach provides the LH source evaluation with much more numerical noise, the pressure Laplacian having similar global structure of sources exhibits a high variability of local structures. Thus the gradient reconstruction technique is further used for LH sound sources computations.

Second, the sound sources computed for three different approaches – the LH analogy, the PCWE and the AWE approaches, are displayed in Figure 13. In the LH case the sound sources are primarily associated with the velocity gradients and in the current simulation they are greatly distributed downstream of glottis and at locations of the glottal jet separation from the VF surface. The dominant sound sources in the cases of the PCWE and the AWE approach are connected with pressure time changes, which local extremes are located primarily in the vortex centers. The PCWE sound sources have a more significant contribution within the glottis. Results of papers [39] and [31] resemble our findings.

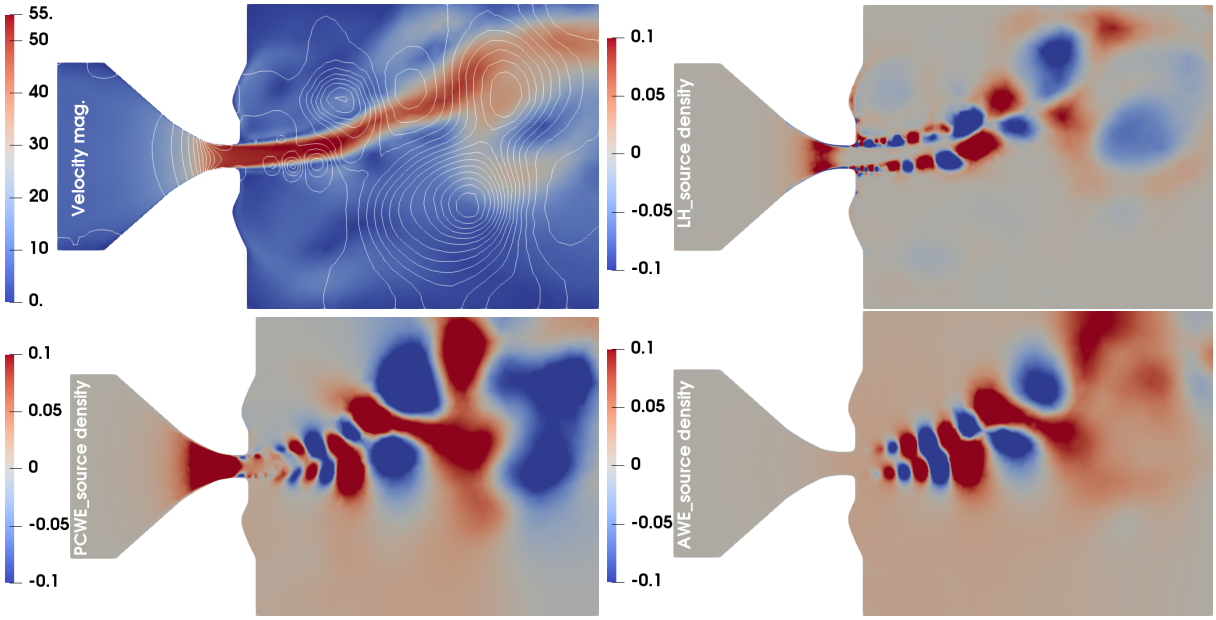

Figure 13: Comparison of instant (normalized) sound densities for different aeroacoustic approaches at time instant 0.6 s. **0)** The magnitude of airflow velocity together with pressure contours. Below the instant sound densities are shown for: **a)** the LH analogy, **b)** the PCWE and **c)** the AWE approach.

Frequency content. The frequency content of the sound sources can be investigated with the aid of the Fourier transform applied on the time signal at each point of the sound sources. The dipole sound source structure can be observed for frequencies of the dominant VF vibration and the quadrupole structure for higher nonharmonic frequencies, see [2].

Sound propagation in the vocal tract model

The sound sources, which were interpolated on the acoustic mesh, are further employed for the LH, the simplified PCWE (sPCWE) and the AWE aeroacoustic simulations within the VT model M2. The speed of sound is considered as $c_0 = 343\,\mathrm{m/s}$ and time step $\Delta t = 0.025\,\mathrm{ms}$ is kept constant. The acoustic pressures are monitored at the same microphone position C as before.

The sound pressure levels computed at point C using all three aeroacoustic approaches are shown in Figure 14. In the frequency range up to 3 kHz all three approaches detect four frequency peaks matching very well the first four formants of the VT model M2. However for the LH case the SPL reaches the highest value of circa 135 dB dominated by frequency peaks at 278 Hz. The sPCWE and AWE approaches provides almost indistinguishable results. Both these approaches are able to predict all four formants with more equal distribution of SPL reaching circa 110 dB. This is in agreement with [39] (see pg. 133), where the SPL of the LH simulation also found to be clearly dominated by the first frequency peak and for the PCWE and the AWE results a very tiny SPL difference ($< 1\,\mathrm{dB}$) was observed.

A similar SPL difference of approximately by 20 dB higher SPL of LH approach (total SPL circa 90 dB) than in the PCWE case reaching approx. 70 dB was obtained by the 3D numerical simulation, see [48]. Further, we regard in agreement with authors of [48] the SPL results of LH analogy as overestimated due to not performed the acoustic/hydrodynamic splitting resulting in the superimposition of hydrodynamic quantities in the sound sources represented by Lighthill tensor. The high values of SPL are probably caused first by a generally different 2D fluid flow dynamics contrary to more complex 3D fluid flow dynamics. Second there are the fundamental differences in wave propagation for 2D formulation compared to 3D setup. Similar aeroacoustic studies of the 2D flow-induced VF vibrations reached comparable high levels of SPL, see [60], [33]. In the end comparing the presented vibroacoustic and aeroacoustic simulations, where the aerodynamically generated sound was about 100 dB higher in SPL than the sound of the vibroacoustic origin (see Fig. 12), it can be concluded that the aerodynamically produced sound is a major sound source of human phonation mechanism in the case without contact of VFs.

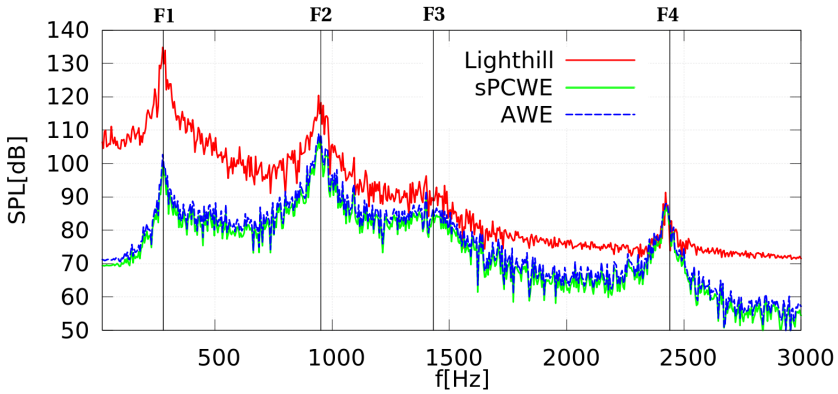

Figure 14: Sound pressure levels of acoustic pressure in frequency domain obtained by the LH analogy, the sPCWE and the AWE approaches at point C. The black vertical lines mark the formants of vocal tract model M2.

7 Conclusion

The first part of the thesis presents the FSI problem in a channel with deformable walls conveying fluid. The mathematical formulation of FSI problem is based on the linear elasticity model and the viscous incompressible Navier-Stokes equations written in the ALE formulation in order to take into account the time-dependence of the flow domain. The numerical approximation of the FSI problem is performed with the FEM in space and the finite difference method in time. Particularly, the fluid flow stabilization, the computation of aerodynamic forces and the construction of ALE mapping is described in detail. The strongly coupled partitioned algorithm is implemented for the solution of the FSI problem. Further, a special attention is paid to the penalization inlet boundary condition which allows to relax an exact value of the inlet velocity at the inlet boundary during channel closing phase. The sensitivity of flow characteristics and critical flutter velocity in dependence on the change of the penalization parameter is investigated.

The FSI results modelling the human phonation are presented, which were achieved with a 2D geometry model of VF. This setting of the FSI problem allows to determine the flutter velocity, to compute flow rate, to evaluate pressure distribution along the whole channel, to investigate the VF vibration shapes, to analyze the energy transfer between vibrating vocal fold and flow, etc.

The second part of the thesis is devoted to the mathematical modelling of acoustic problems connected with the human phonation. Two models of sound production are described, namely the vibroacoustic problem studies sound produced solely by vibrating boundary of structure (e.g. VFs), and the aeroacoustic problem deals with generation and propagation of the sound with aerodynamic origin. The aeroacoustic part is addressed using the hybrid approach. It allows to predict sound based on the incompressible flow simulation, i.e. to use more appropriate and computationally less demanding acoustic solver than the solver of compressible flow and to simulate acoustic problem in larger domains.

The main novelty of the presented aeroacoustic approach is given by the connection between the FSI simulation with apriori unknown structure motion excited by the airflow and the acoustics solved in the acoustic propagation domain with included vocal tract model. This setting enables to obtain relevant aeroacoustic results.

The frequency characteristics of several vocal tract models were investigated in order to identify first formants. The lowest four formants were obtained by the numerical solution of the Helmholtz equation in a 2D vocal tract with the considered PML technique modelling the radiation outside mouth and with the sound hard BC applied at boundaries of given vocal tract model. The determined formants match the laboratory measured formants in an acceptable way.

The vibroacoustic simulation presents the results of the sound propagation excited by the VF walls vibration. In the acoustic spectra it is clearly visible the first two eigenfrequencies of VF model together with formants of chosen vocal tract model. The resulting SPL composed of relevant acoustic frequency spectrum is considerably low in comparison with the SPL of aerodynamically produced sound.

Finally, the aeroacoustic simulations comprise the sound sources evaluation, the sound sources interpolation on the acoustic grid and the sound sources propagation through the vocal tract model. As the sound sources computation is of key importance a special care is paid to the sound source numerical computation including a few alternative sound source formulations. The computed sound sources are qualitatively compared. The sound propagation results compare three different approaches, namely the LH analogy, the simplified PCWE and the AWE approach. The sound signals outside the mouth have frequency spectra consisting of all four formants of the used vocal tract model. The resulting SPL of LH analogy obviously overestimates the lower

frequencies. The sPCWE and the AWE approaches provide almost the same acoustic results having more uniform spectral distribution.

Achieved results

The objectives of the dissertation as they were formulated in Introduction are achieved, namely:

- The behaviour of new penalization inlet boundary condition was described for the internal aerodynamics configurations when the channel is closing. The closing channel up to the half-gap value of 10 μm with reasonable pressure values was demonstrated for the VF prescribed motion in Chapter 5 indicating a promising way towards the modelling of the complete channel closure.
- The methodology how to find the stability boundary of the modelled aeroelastic system was developed for the classical Dirichlet BC and also for a wide range of penalization parameters.
- The connection between the in-house solver FSIFEM and the academic solver CFS++ of TU Vienna was establishedthrough the file format HDF5.
- A special attention was paid to the sound sources computation. For the LH analogy the numerical procedure based on the local reconstruction technique was proposed and further its applicability was shown.
- The aeroacoustic simulations were performed by using the three different aeroacoustic approaches. The corresponding sound sources were analyzed and the sound spectra in front of the mouth were compared.
- The simulated sound of the vibroacoustic origin was found quite low suggesting to be relatively insignificant sound source in human phonation (at least for the presented FSI simulation without complete closure of the glottis and the VFs collision).

Research outlook. The developed computational model of the FSAI problem has demonstrated the capability to simulate the complex flow-induced VF vibrations and the produced vibroacoustic and aeroacoustic sound. In the near future, I would like to extended the work in several directions:

- Aeroacoustics based on the FSI simulation with penalization BC at the inlet. Some very preliminary results were already presented at *Workshop: Strömungsschall in Luftfahrt, Fahrzeug- und Anlagentechnik, 2019.*
- Implementation/improvement of glottal channel closure based on the presented FSI model together with the penalty inlet boundary condition.
- Modelling of contact during vocal folds collisions. For a general VF shape it can be quite difficult task due to need of finding contact points on the interface represented by a general curve and further to calculate the contact force at each relevant point of the VF tissue.

Reference

Author's publications

[1] *FSIFEM*, https://github.com/jvalasek/FSIfem/, 1.6.2019 [software].

[2] J. Valášek, M. Kaltenbacher, and P. Sváček, *On the application of acoustic analogies in the numerical simulation of human phonation process*, Flow, Turbulence and Combustion, 2019, pp. 129–143.

[3] J. Valášek, P. Sváček, and J. Horáček, *Numerical solution of fluid-structure interaction represented by human vocal folds in airflow*, EFM15, EPJ Web of Conferences, 2016.

[4] J. Valášek, P. Sváček, and J. Horáček, *On suitable inlet boundary conditions for fluid-structure interaction problems in a channel*, Applications of Mathematics **64**:2 (2019), 225–251.

[5] J. Valášek, P. Sváček, and J. Horáček, *Fluid-structure-acoustic interaction problem in modelling of human vocal folds vibration*, Proceedings of the Conference Algoritmy 2020 (Frolkovič, Mikula, and Ševčovič., eds.), Slovak University of Technology in Bratislava, 2020, pp. 81–90.

[6] J. Valášek, P. Sváček, and J. Horáček, *The flow-induced vibrations of vocal folds approximated by the finite element method*, , Lecture Notes in Mechanical Engineering, Springer, 2021, pp. 377–388.

[7] J. Valášek, P. Sváček, and J. Horáček, *Numerical approximation of fluid-structure interaction problem in a closing channel near the stability boundary*, Numerical Mathematics and Advanced Applications ENUMATH 2019 (F. Vermolen and C. Vuik, eds.), Lecture Notes in Computational Science and Engineering, vol. 139, Springer International Publishing, 2021.

[8] J. Valášek, M. Kaltenbacher, and P. Sváček, *The comparison of different acoustic approaches in the simulation of human phonation*, Coupled Problems in Science and Engineering VII (E. O. Manolis Papadrakakis and B. Schrefler, eds.), 2017, pp. 661–672.

[9] J. Valášek, P. Sváček, and J. Horáček, *The influence of different geometries of human vocal tract model on resonant frequencies*, Topical problems of fluid mechanics 2018 (D. Šimurda and T. Bodnár, eds.), Institute of Thermomechanics, AS CR, 2018, pp. 307–314.

[10] J. Valášek, P. Sváček, and J. Horáček, *Aerodynamic transfer of energy to vibrating vocal folds for different driving mechanisms*, Topical problems of fluid mechanics 2019 (D. Šimurda and T. Bodnár, eds.), Institute of Thermomechanics, AS CR, 2019, pp. 197–204.

[11] J. Valášek, M. Kaltenbacher, and P. Sváček, *The application of Lighthill analogy on the numerical simulation of human phonation*, Topical problems of fluid mechanics 2017 (D. Šimurda and T. Bodnár, eds.), Institute of Thermomechanics, AS CR, 2017, pp. 303–312.

[12] J. Valášek, P. Sváček, and J. Horáček, *The numerical simulation of human phonation*, Computational Mechanics 2018 – Book of Extended Abstracts, University of West Bohemia, pp. 127–128.

[13] J. Valášek, P. Sváček, and J. Horáček, *The influence of penalization inlet boundary condition on the stability boundary*, Proceedings of Computational Mechanics 2019, University of West Bohemia, 2019, pp. 212–215.

[14] J. Valášek, P. Sváček, and J. Horáček, *The investigation of acoustical signal induced by vibrations of human vocal folds*, Studentská tvůrčí činnost 2018 - sborník konference (J. Moravec, ed.), České vysoké učení technické v Praze, Fakulta strojní, apr 2018.

Bibliography

[15] I. Babuška, T. Strouboulis, S. Gangaraj, and C. Upadhyay, *Validation of recipes for the recovery of stresses and derivatives*, Mathematical and computer modelling **20**:6 (1994), 45–89.

[16] I. Babuška, *The finite element method with penalty*, Mathematics of Computation, 1973, 221–228.

[17] S. Badia, F. Nobile, and C. Vergara, *Fluid–structure partitioned procedures based on Robin transmission conditions*, Journal of Computational Physics **227**:14 (2008), 7027–7051.

[18] Y. Bae and Y. J. Moon, *Computation of phonation aeroacoustics by an INS/PCE splitting method*, Computers & Fluids **37** (2007), 1332 – 1343.

[19] M. Braack and P. B. Mucha, *Directional do-nothing condition for the Navier-Stokes equations*, Journal of Computational Mathematics **32** (2014), 507–521.

[20] M. Brdička, L. Samek, and B. Sopko, *Continuum mechanics*, Academia, 2000.

[21] D. J. Daily and S. L. Thomson, *Acoustically-coupled flow-induced vibration of a computational vocal fold model*, Computers & Structures **116** (2013), 50–58.

[22] R. Ewert and W. Schröder, *Acoustic perturbation equations based on flow decomposition via source filtering*, Journal of Computational Physics **188**:2 (2003), 365–398.

[23] M. Feistauer, P. Sváček, and J. Horáček, *Numerical simulation of fluid-structure interaction problems with applications to flow in vocal folds*, Fluid-structure Interaction and Biomedical Applications (T. Bodnár, G. P. Galdi, and S. Nečasová, eds.), Birkhauser, 2014, pp. 312–393.

[24] C. Föster, *Robust methods for fluid-structure interaction with stabilised finite elements*, Ph.D. thesis, Institut fuer Baustatik und Baudynamik der Universitaet Stuttgart, 2007.

[25] T. Gelhard, G. Lube, M. Olshanskii, and J.-H. Starcke, *Stabilized finite element schemes with LBB-stable elements for incompressible flows*, Journal of Computational and Applied Mathematics **177**:2 (2005), 243–267.

[26] V. Girault and P. A. Raviart, *Finite element methods for Navier-Stokes equations*, 1986.

[27] J. Horáček, V. V. Radolf, V. Bula, and J. Košina, *Experimental modelling of phonation using artificial models of human vocal folds and vocal tracts*, Engineering Mechanics 2017 (V. Fuis, ed.), Brno University of Technology, FME, 2017, pp. 382–385.

[28] J. Horáček, V. V. Radolf, and A.-M. Laukkanen, *Experimental and computational modeling of the effects of voice therapy using tubes*, Journal of Speech, Language, and Hearing Research, American Speech-Language-Hearing Association, 2019, pp. 1–18.

[29] J. Horáček, P. Šidlof, and J. Švec, *Numerical simulation of self-oscillations of human vocal folds with Hertz model of impact forces*, Journal of Fluids and Structures **20**:6 (2005), 853 – 869.

[30] M. S. Howe, *Acoustics of fluid-structure interactions*, Cambridge University Press, 1998.

[31] A. Hüppe, *Spectral finite elements for acoustic field computation*, Ph.D. thesis, Alpen-Adria-Universität Klagenfurt, 2012.

[32] M. Kaltenbacher, M. Escobar, S. Becker, and I. Ali, *Numerical simulation of flow-induced noise using LES/SAS and Lighthill's acoustic analogy*, International Journal for Numerical Methods in Fluids **63**:9 (2010), 1103–1122.

[33] M. Kaltenbacher, S. Zörner, and A. Hüppe, *On the importance of strong fluid-solid coupling with application to human phonation*, Progress in Computational Fluid Dynamics **14**:1 (2014), 2–13.

[34] M. Kaltenbacher, *Numerical simulation of mechatronic sensors and actuators: finite elements for computational multiphysics*, Springer, 2015.

[35] A. Kosík, *Fluid-structure interaction*, Ph.D. thesis, MFF, Charles University in Prague, 2016.

[36] M. Lasota, P. Šidlof, M. Kaltenbacher, and S. Schoder, *Impact of the sub-grid scale model in aeroacoustic simulation of human voice*, Applied Sciences (to appear) (2021).

[37] M. J. Lighthill, *On sound generated aerodynamically. I. General theory*, Proceedings of the Royal Society of London, vol. 211, The Royal Society, 1952, pp. 564–587.

[38] G. Link, M. Kaltenbacher, M. Breuer, and M. Döllinger, *A 2D finite-element scheme for fluid-solid-acoustic interactions and its application to human phonation*, Computer Methods in Applied Mechanics and Engineering **198** (2009), 3321 – 3334.

[39] M. A. Lodermeyer, *A laser-based technique to evaluate sound generation during phonation*, Ph.D. thesis, Friedrich-Alexander-Universität Erlangen-Nürnberg, 2019.

[40] R. Mittal, B. D. Erath, and M. W. Plesniak, *Fluid dynamics of human phonation and speech*, Annual Review of Fluid Mechanics **45** (2013), 437–467.

[41] J. Niu, J. Lei, and J. He, *Radial basis function mesh deformation based on dynamic control points*, Aerospace Science and Technology **64** (2017), 122 – 132.

[42] M. de Oliveira Rosa, J. C. Pereira, M. Grellet, and A. Alwan, *A contribution to simulating a three-dimensional larynx model using the finite element method*, The Journal of the Acoustical Society of America **114**:5 (2003), 2893–2905.

[43] H. Sadeghi, M. Döllinger, M. Kaltenbacher, and S. Kniesburges, *Aerodynamic impact of the ventricular folds in computational larynx models*, JASA **145**:4 (2019), 2376–2387.

[44] S. Schoder and M. Kaltenbacher, *Hybrid aeroacoustic computations: State of art and new achievements*, Journal of Theoretical and Computational Acoustics (2020).

[45] S. Schoder, K. Roppert, M. Weitz, C. Junger, and M. Kaltenbacher, *Aeroacoustic source term computation based on radial basis functions*, International Journal for Numerical Methods in Engineering (2019).

[46] B. Schott, C. Ager, and W. A. Wall, *A monolithic approach to fluid-structure interaction based on a hybrid Eulerian-ALE fluid domain decomposition involving cut elements*, International Journal for Numerical Methods in Engineering **119**:3 (2019), 208–237.

[47] J. H. Seo and R. Mittal, *A high-order immersed boundary method for acoustic wave scattering and low-Mach number flow-induced sound in complex geometries*, Journal of Computational Physics **230**:4 (2011), 1000–1019.

[48] P. Šidlof, S. Zörner, and A. Hüppe, *A hybrid approach to the computational aeroacoustics of human voice production*, Biomechanics and Modeling in Mechanobiology **14**:3 (2014), 473–488.

[49] B. H. Story, I. R. Titze, and E. A. Hoffman, *Vocal tract area functions from magnetic resonance imaging*, The Journal of the Acoustical Society of America **100**:1 (1996), 537–554.

[50] J. Suh and S. H. Frankel, *Numerical simulation of turbulence transition and sound radiation for flow through a rigid glottal model*, The JASA **121**:6 (2007), 3728–3739.

[51] P. Sváček and J. Horáček, *Numerical simulation of glottal flow in interaction with self oscillating vocal folds: comparison of finite element approximation with a simplified model*, Communications in Computational Physics **12** (2012), 789–806.

[52] ———, *Finite element approximation of flow induced vibrations of human vocal folds model: Effects of inflow boundary conditions and the length of subglottal and supraglottal channel on phonation onset*, Applied Mathematics and Computation **319** (2018), 178–194.

[53] N. Takashi and T. J. R. Hughes, *An arbitrary Lagrangian-Eulerian finite element method for interaction of fluid and a rigid body*, Computer Methods in Applied Mechanics and Engineering **95** (1992), 115–138.

[54] S. L. Thomson, L. Mongeau, and S. H. Frankel, *Aerodynamic transfer of energy to the vocal folds*, The Journal of the Acoustical Society of America **118**:3 (2005), 1689–1700.

[55] I. R. Titze, *The physics of small-amplitude oscillation of the vocal folds*, The Journal of the Acoustical Society of America **83**:4 (1988), 1536–1552.

[56] I. R. Titze, *Principles of voice production*, Prentice Hall, 1994.

[57] I. R. Titze, *Nonlinear source–filter coupling in phonation: Theory*, The Journal of the Acoustical Society of America **123**:4 (2008), 1902–1915.

[58] Q. Xue, X. Zheng, R. Mittal, and S. Bielamowicz, *Subject-specific computational modeling of human phonation*, The Journal of the Acoustical Society of America **135**:3 (2014), 1445–1456.

[59] W. Zhao, C. Zhang, S. H. Frankel, and L. Mongeau, *Computational aeroacoustics of phonation, part I: Computational methods and sound generation mechanisms*, The Journal of the Acoustical Society of America **112**:5 (2002), 2134–2146.

[60] S. Zörner and M. Kaltenbacher, *Fluid-structure-acoustic interaction algorithms and implementations using the finite element method*, Eccomas, vol. 2010, 2010, p. 28.

[61] S. Zörner, M. Kaltenbacher, and M. Döllinger, *Investigation of prescribed movement in fluid-structure interaction simulation for the human phonation process*, Computers & Fluids, 2013.

Summary

The first part of dissertation thesis deals with the numerical simulation of the fluid-structure interaction (FSI) in 2D modelling the vocal folds vibration excited by airflow. The vocal fold (VF) deformation is described by the linear elasticity model and the flow is modelled by the incompressible Navier-Stokes equations in the arbitrary Lagrangian-Eulerian (ALE) formulation in order to take into account the time-dependence of the flow domain. The space discretization of both subproblems is realized by the finite element method (FEM) and the Newmark method for the structure time discretization is applied while the fluid flow problem is approximated in time by the BDF2 method. A special attention is paid to the fluid flow stabilization, to the calculation of aerodynamic forces and to the airflow inlet boundary conditions at the entrance to the glottal channel. The penalization boundary condition is compared with the Dirichlet and the do-nothing boundary condition and its advantages are shown for solving of the internal aerodynamics configurations when the channel is closing. Particularly, the dependence of critical flutter airflow velocity on the penalization parameter is determined and the energy transfer between airflow and the vibrating elastic body is analyzed.

The second part of thesis extended FSI problem to the interaction of fluid flow, an elastic body and acoustics. It addresses the aeroacoustic and the vibroacoustic problems motivated by human phonation. The presented hybrid aeroacoustic approaches allows to predict sound based on the incompressible flow simulation, i.e. acoustic computation has the form of the FSI results postprocessing. Alternative sound source formulations and their numerical implementations are described and applied in several investigated cases. The frequency characteristics of considered vocal tract (VT) models with perfectly matched layer technique at the VT end representing open-boundary condition are determined by solving the Helmholtz equation. The computed sound of vibroacoustic origin, i.e. excited purely by the VF vibration, reaches significantly lower sound pressure levels (SPL) than the sound of aeroacoustic origin. The aeroacoustic simulations comprise the sound sources evaluation in the computed airflow pattern, the sound sources interpolation on the acoustic grid and finally modelling of the sound sources transient propagation in the VT. Three different approaches – namely the Lighthill analogy (LH), the (simplified) perturbed convective wave equation (sPCWE) and the aeroacoustic wave equation (AWE), are compared. The SPL show overestimation in the case of LH and almost identical results of sPCWE and AWE. In all cases the excited spectra of acoustic pressures are dominated by the acoustic resonances (formants) of the vocal tract model.

Key words:
Fluid-structure interaction, fluid-structure-acoustic interaction, linear elasticity, incompressible fluid flow, Navier-Stokes equations, Lighthill acoustic analogy, perturbed convective wave equation, aeroacoustic wave equation, finite element method, ALE method, perfectly-matched layer, human phonation modelling.

Resumé

První část dizertační práce se zabývá numerickou simulací interakce proudící tekuitny a elastického tělesa (FSI) v 2D modelování vibrace lidských hlasivek vybuzených prouděním vzduchu. Deformace lidských hlasivek je popsána pomocí lineárního elastického modelu a proudění tekutiny je modelováno nestlačitelnými Navierovými-Stokesovými rovnicemi v ALE formulaci, která umožňuje zahrnout efekty časově proměnné oblasti proudění. Prostorová diskretizace obou podúloh je realizována metodou konečných prvků (FEM) a pro časovou diskretizaci elastického tělesa je použita Newmarkova metoda, zatímco problém proudění je aproximován v čase pomocí metody BDF2. Specialní pozornost je věnována stabilizaci FEM pro aproximaci proudění, výpočtu aerodynamických sil a okrajovým podmínkám předepsaným na vstupu do glotálního kanálu. Je porovnána penalizační okrajová podmínka s Dirichletovou a do-nothing okrajovou podmínkou, a jsou ukázány její výhody pro řešení konfigurací vnitřní aerodynamiky, kdy dochází k uzavírání kanálu. Zejména je určena závislost kritické flutterové rychlosti proudění na penalizačním parametru a dále je analyzován přenos energie mezi prouděním tekutiny a kmitajícím elastickým tělesem.

V druhé části dizertace je FSI problém rozšířen na problém na interakce proudící tekutiny, elastické struktury a akustiky. Tento problém zahrnuje popis aeroakustických a vibroakustických úloh motivovaných modelováním lidské fonace. Předsta-vený hybridní aeroakustický přístup dovoluje určit zvukovou hladinu na základě simulace nestlačitelného proudění, tj. akustický výpočet má formu postprocesingu výsledků FSI úlohy. Jsou popsány alternativní formulace zvukových zdrojů a jejich numerická implementace v několika vyšetřovaných případech. Frekvenční charakteristika uvažovaného modelu vokálního traktu (VT) s PML metodou použitou na konci VT pro modelování problému s volnou hranicí je určena pomocí řešení Helmholtzovy rovnice. Vypočtený zvuk vibroakustického původu, tj. vybuzený čistě kmitáním hlasivek, dosahuje výrazně nižší zvukové hladiny než zvuk aeroakustického původu. Aeroakustické simulace se skládají z výpočtu zvukových zdrojů na základě výsledků proudění, z interpolace zvukových zdrojů na akustickou síť a ze záverečného modelování postupného šíření těchto zdrojů v čase skrz vokální trakt. Jsou srovnány tři různé přístupy – Lighthillova akustické analogie (LH), (zjednodušená) perturbovaná konvektivní vlnové rovnice (sPCWE) a aeroakustická vlnová rovnice (AWE). Hladina zvuku vykazuje nadhodnocení v případě Lighthillovy analogie a téměř totožné výsledky při použití přístupů sPCWE a AWE. Ve všech případech jsou v získaných akustických spektrech dominantní akustické resonance (formanty) použitého modelu vokálního traktu.

Klíčová slova:
Interakce proudění s elastickým tělesem, interakce proudění a elastického tělesa i akustiky, lineární elasticita, nestlačitelné proudění tekutiny, Navierovy-Stokesovy rovnice, Lighthillova akustická analogie, perturbovaná konvektivní vlnová rovnice, aeroakustická vlnová rovnice, metoda konečných prvků, ALE metoda, PML vrstva, modelování lidské fonace.